

Resonant Reheating

Basabendu Barman,^a Nicolás Bernal,^b Yong Xu^c

^aDepartment of Physics, School of Engineering and Sciences, SRM University-AP
Amaravati 522240, India

^bNew York University Abu Dhabi
PO Box 129188, Saadiyat Island, Abu Dhabi, United Arab Emirates

^cPRISMA⁺ Cluster of Excellence and Mainz Institute for Theoretical Physics
Johannes Gutenberg University, 55099 Mainz, Germany

E-mail: basabendu.b@srmmap.edu.in, nicolas.bernal@nyu.edu, yonxu@uni-mainz.de

Abstract. We investigate a novel reheating scenario proceeding through s -channel inflaton annihilation, mediated by a massive scalar. If the inflaton ϕ oscillates around the minimum of a monomial potential $\propto \phi^n$, we reveal the emergence of resonance phenomena originating from the dynamic evolution of the inflaton mass for $n > 2$. Consequently, a *resonance* appears in both the radiation and the temperature evolution during the reheating process. By solving the coupled Boltzmann equations, we present solutions for radiation and temperature. We find non-trivial temperature characteristics during reheating, depending on the value of n and the masses of the inflaton and mediator. Some phenomenological aspects of the model are explored. As a concrete example, we show that the same mediator participates in the genesis of dark matter, modifying the standard freeze-in dynamics. In addition, we demonstrate that the resonant reheating scenario could be tested by next-generation low- and high-frequency gravitational wave detectors.

Contents

1	Introduction	1
2	Post-inflationary reheating dynamics	2
2.1	Bosonic reheating	4
2.2	Fermionic reheating	8
3	Dark matter freeze-in during resonant reheating	10
3.1	From the thermal bath	11
3.2	From inflaton annihilations	15
3.3	Gravitational production	18
4	Primordial gravitational waves	19
5	Conclusions	22
A	Annihilation to mediators	23

1 Introduction

Cosmic inflation is an elegant paradigm to solve several problems in cosmology [1–4]. In the conventional cosmological narrative, the initially (quasi) exponential expansion leads the Universe to be cold at the end of inflation. Understanding the transition from this state to a hot, thermal, radiation-dominated Universe, laying the foundation for Big Bang nucleosynthesis (BBN), is vital. This heating process not only elucidates the cosmic origins of the matter we observe, but also accounts for relics such as photons, neutrinos, and primordial gravitational waves (GW), along with exotic particles beyond the Standard Model (SM), for instance dark matter (DM).

The basic idea of reheating after inflation is as follows: it occurs due to the production of particles by the oscillating scalar field ϕ [5, 6]. In the most basic inflationary models, this field, responsible for driving inflation, subsequently undergoes oscillations near the minimum of its effective potential $V(\phi) \propto \phi^n$, thus inducing particle production. Reheating can be performed through interactions between the inflaton and some light degrees of freedom. Such interactions, which result in energy transfer from the inflaton to the SM fields, can proceed through inflaton decays, for example, as discussed in Refs. [7–9] or inflaton scattering [10, 11].¹

In the case of reheating through inflaton annihilations, contact interactions between a pair of inflatons and a pair of SM particles are typically assumed. Inflaton annihilations through a mediator have been studied in the framework of gravity, where the graviton plays the role of mediator. However, it has been shown that rather steep inflaton potentials with $n > 9$ are needed for successful reheating [17–21]. Interestingly, this bound can be relaxed to $n > 4$ if one introduces a non-minimal coupling between gravity and a pair of inflatons [22], or even to $n \geq 2$ if gravity couples non-minimally to a single inflaton [23].

¹The effect of time-dependent inflaton decay on reheating dynamics has been discussed in, for example, Refs. [12–16].

In this work, however, we investigate a previously unexplored novel possibility of reheating through scalar-mediated s -channel scattering. In particular, we consider a model in which a pair of inflatons (ϕ) annihilate into a pair of daughter particles through the s -channel exchange of a massive spin-0 mediator (S). The daughter particles could be Higgs bosons in the SM or particles beyond the SM like right-handed neutrinos. If the inflaton oscillates in a potential steeper than that of the quadratic, the inflaton mass is not a constant but decreases with time. Consequently, the existence of higher modes can give enough energy to the inflaton so that mediators are produced *resonantly*. Once these mediator fields are produced, they quickly decay into SM particles that make up the thermal bath. Because of the resonant production of the mediator, the evolution of the SM temperature features non-trivial behavior (typically a bump) during reheating, which is very different from the standard cases characterized by a simple power law. We find that in the presence of a resonance, the maximum temperature during reheating is controlled by the location of the resonance relative to the end of the reheating. In particular, when the resonance occurs close to the end of reheating, the reheating temperature would be the maximum temperature and can be larger than that where the resonance is absent.

Interestingly, the mediator S could also play a fundamental role in the production of particles beyond the SM, such as the DM. In particular, if the DM has very suppressed couplings with the SM so that it never reaches thermal equilibrium, it can be produced in the early Universe through the FIMP mechanism [24–29]. The dynamics of reheating determines the abundance of DM if it is produced *during* reheating, and in that case it is called an ultraviolet (UV) FIMP [30–32]. We further explore the impact of such a resonant reheating on DM production from the visible sector or inflaton, mediated by S or graviton. We find that new and interesting freeze-in behaviors show up mainly due to the presence of the resonance feature during reheating.

Primordial gravitational waves (GW) serve as a robust prediction for inflationary models. In the course of inflation, quantum fluctuations inevitably lead to a spectrum of tensor-metric perturbations on scales beyond the Hubble horizon. In a conventional post-inflationary scenario, these tensor modes transition to subhorizon scales during the radiation-dominated epoch. However, it is widely recognized that the presence of nonstandard cosmological conditions, such as an early stiff era preceding radiation domination, disrupts this scale invariance [33]. Under such circumstances, the GW spectrum experiences a significant blue tilt within the frequency range corresponding to the modes that cross the horizon during the stiff period [34–50]. Such a blue-tilted spectrum turns out to be well within the reach of several GW detector facilities. Our scenario turns out to be testable on several next-generation GW detectors.

The paper is organized as follows. In Section 2, we offer the model setup and explore the features of resonance reheating with both numerical results and analytical approximations. In Section 3, we investigate the implications for the production of DM due to the presence of resonance. Section 4 is devoted to discussions of the testability of the present framework with the primordial GW spectrum. We sum up our findings in Section 5.

2 Post-inflationary reheating dynamics

After the end of cosmic inflation, inflatons oscillate around the minimum of their potential, transferring energy to SM particles that subsequently thermalize, forming the SM thermal bath. We consider the post-inflationary oscillation of the inflaton ϕ at the bottom of a

monomial potential $V(\phi)$ of the form

$$V(\phi) = \lambda \frac{\phi^n}{M_P^{n-4}}, \quad (2.1)$$

where λ is a dimensionless coupling and $M_P \simeq 2.4 \times 10^{18}$ GeV the reduced Planck mass. This type of potential could arise from α -attractor T - or E -models [51, 52], or the Starobinsky inflationary model [1, 53–55]. Defining the energy density and pressure of ϕ as $\rho_\phi \equiv \frac{1}{2} \dot{\phi}^2 + V(\phi)$ and $p_\phi \equiv \frac{1}{2} \dot{\phi}^2 - V(\phi)$, the background equation-of-state parameter is defined as $w \equiv p_\phi/\rho_\phi = (n-2)/(n+2)$ [56]. For example, for $n = 4$, $w = 1/3$ corresponding to a radiation-like background.

The evolution of the energy densities of the inflaton ρ_ϕ and the SM radiation ρ_R can be tracked using the Boltzmann equations²

$$\frac{d\rho_\phi}{dt} + \frac{6n}{2+n} H \rho_\phi = -\frac{2n}{2+n} \Gamma^{2 \rightarrow 2} \rho_\phi \quad (2.2)$$

$$\frac{d\rho_R}{dt} + 4H \rho_R = +\frac{2n}{2+n} \Gamma^{2 \rightarrow 2} \rho_\phi, \quad (2.3)$$

where

$$H = \sqrt{\frac{\rho_R + \rho_\phi}{3M_P^2}}, \quad (2.4)$$

is the Hubble expansion rate, and $\Gamma^{2 \rightarrow 2}$ the 2-to-2 annihilation rate of a pair of inflaton condensate into a pair of SM states. The detailed expression of $\Gamma^{2 \rightarrow 2}$ will be discussed in a moment.

During reheating, that is, when $a_I \leq a \leq a_{\text{rh}}$, where a is the cosmic scale factor, the expansion H dominates over the interaction $\Gamma^{2 \rightarrow 2}$, and then

$$\rho_\phi(a) \simeq \rho_\phi(a_I) \left(\frac{a_I}{a}\right)^{\frac{6n}{2+n}}. \quad (2.5)$$

Here, a_I and a_{rh} correspond to the scale factor at the end of inflation (that is, at the beginning of reheating) and at the end of reheating, respectively. Since the Hubble rate during reheating is dominated by the inflaton energy density, it follows that

$$H(a) \simeq H(a_{\text{rh}}) \times \begin{cases} \left(\frac{a_{\text{rh}}}{a}\right)^{\frac{3n}{n+2}} & \text{for } a_I \leq a \leq a_{\text{rh}}, \\ \left(\frac{a_{\text{rh}}}{a}\right)^2 & \text{for } a_{\text{rh}} \leq a, \end{cases} \quad (2.6)$$

taking into account that after the end of reheating the Hubble expansion rate is dominated by free SM radiation.

The effective mass m_ϕ of the inflaton can be obtained from the second derivative of Eq. (2.1), which reads [62]

$$m_\phi^2(a) \equiv \frac{d^2V}{d\phi^2} = n(n-1) \lambda M_P^2 \left(\frac{\phi}{M_P}\right)^{n-2} \simeq n(n-1) \lambda^{\frac{2}{n}} M_P^2 \left(\frac{\rho_\phi(a)}{M_P^4}\right)^{\frac{n-2}{n}}. \quad (2.7)$$

²We also assume that the thermalization of the SM plasma occurs instantaneously. We note, however, that the SM particles do not necessarily thermalize suddenly, and thus they could be initially distributed with smaller occupation numbers and harder momenta [57–61].

In the last step, we have considered $\rho_\phi \simeq V(\phi)$ and utilized the relation between the inflaton field ϕ and the potential given in Eq. (2.1). The inflaton mass at a scale factor a can be related to its value $m_I \equiv m_\phi(a_I)$ at the beginning of the reheating by

$$m_\phi(a) \simeq m_I \left(\frac{a_I}{a} \right)^{\frac{3(n-2)}{n+2}}. \quad (2.8)$$

It is interesting to note that for $n \neq 2$, m_ϕ has a field dependence that will be inherited by the interaction rate $\Gamma^{2 \rightarrow 2}$. Additionally, for $n = 2$, radiation cannot exceed the inflaton energy density, and therefore reheating is not viable if it proceeds through annihilations with $n < 5/2$ [11].³ In the following, we will therefore focus on the case $n \geq 4$.

2.1 Bosonic reheating

As advocated in the beginning, here we are interested in the 2-to-2 scattering of the inflaton $\phi\phi \rightarrow S \rightarrow hh$, mediated by a real singlet scalar S in the s channel.⁴ This can arise from an effective Lagrangian density interaction of the form

$$\mathcal{L} \supset \frac{1}{2} \tilde{\mu}_\phi \phi^2 S + \frac{1}{2} \mu_h S h^2, \quad (2.9)$$

where ϕ is the inflaton field, S is the mediator and h a SM-like field.⁵ Note that both couplings have a mass dimension. Since the inflaton oscillates in a monomial potential, one must take care of the Fourier modes of the annihilating inflaton field. In that case, after averaging over several oscillations, the scattering rate for $\phi\phi \rightarrow S \rightarrow hh$ turns out to be

$$\Gamma^{\phi\phi \rightarrow hh} \simeq \frac{\rho_\phi}{m_\phi} \frac{\mu_\phi^2 \mu_h^2}{32\pi m_\phi^2 \left[(4m_\phi^2 - m_s^2)^2 + \Gamma_s^2 m_s^2 \right]} \sqrt{1 - \frac{m_h^2}{m_\phi^2}} \Theta(m_\phi - m_h), \quad (2.10)$$

where S has a mass m_s and a total decay width

$$\Gamma_s = \frac{1}{8\pi} \frac{\mu_h^2}{m_s} \sqrt{1 - \frac{4m_h^2}{m_s^2}} \Theta(m_s - 2m_h) + \frac{1}{8\pi} \frac{\mu_\phi^2}{m_s} \sqrt{1 - \frac{4m_\phi^2}{m_s^2}} \Theta(m_s - 2m_\phi), \quad (2.11)$$

with Θ being the Heaviside step function. Here, the *effective* coupling μ_ϕ is proportional to $\tilde{\mu}_\phi$ and encodes the summation over several oscillations of Fourier modes [10, 62–66]. It is interesting to note that the rate in Eq. (2.10) features a pole when $m_\phi(a) = m_s/2$. As the inflaton mass varies during reheating, this resonance could be reached. It occurs at the scale factor a_p given by

$$a_p \equiv a_I \left(\frac{2m_I}{m_s} \right)^{\frac{2+n}{3(n-2)}}. \quad (2.12)$$

³Reheating through annihilations and $n = 2$ could become viable in the case of an inflaton *nonminimally* coupled to gravity [23].

⁴We note that if $\phi\phi \rightarrow S \rightarrow hh$ is present, one can not avoid the annihilation $\phi\phi \rightarrow SS$ through t and u channels. Subsequently, the mediators S decay into a pair of SM particles $S \rightarrow hh$. However, in the present setup, this channel is subdominant, as explored in Appendix A.

⁵We assume quartic interaction terms, e.g., $\phi^2 S^2$, $S^2 h^2$, $\phi^2 h^2$ or trilinear interaction between the inflaton and a pair of SM Higgs ϕh^2 , are absent. We remain agnostic about the UV completion of our effective toy model.

We emphasize that here we are interested in the case where $n \geq 4$. Additionally, we will focus on the case where the resonance is reached during the reheating era.

This system of Boltzmann equations (2.2) and (2.3) can be solved analytically. Taking the initial conditions at $a = a_I$ to be $\rho_R(a_I) = 0$ and $\rho_\phi(a_I) = 3 H_I^2 M_P^2$, with H_I being the inflationary scale,⁶ the SM energy density can be approximated by

$$\rho_R(a) \simeq \frac{H_I^3 M_P^4 \mu_h^2 \mu_\phi^2}{m_I^7} \times \begin{cases} \frac{9}{512\pi} \frac{n}{8n-17} \left(\frac{a}{a_I}\right)^{\frac{6(2n-7)}{2+n}} \left[1 - \left(\frac{a_I}{a}\right)^{\frac{2(8n-17)}{n+2}}\right] & \text{for } a_I \leq a \ll a_p, \\ \frac{3\pi}{2} \frac{n}{n-2} \left(\frac{a_I}{a}\right)^4 \left(\frac{2m_I}{m_s}\right)^{\frac{n-4}{3(n-2)}} \frac{m_I^5}{m_s^3 \mu_h^2} & \text{for } a_p \lesssim a \lesssim a_t, \\ \frac{9}{32\pi} \frac{n}{2n-5} \left(\frac{a_I}{a}\right)^{\frac{18}{n+2}} \left[1 - \left(\frac{a_I}{a}\right)^{\frac{2(2n-5)}{2+n}}\right] \left(\frac{m_I}{m_s}\right)^4 & \text{for } a_t \lesssim a \leq a_{\text{rh}}. \end{cases} \quad (2.13)$$

Finally, after the end of the reheating, when $a > a_{\text{rh}}$, the SM radiation scales as free radiation and therefore $\rho_R(a) \propto a^{-4}$. Some comments on the analytical solution in Eq. (2.13) are in order: *i*) before the resonance, that is, for $a_I \leq a \ll a_p$, the terms proportional to Γ_s and m_s in the denominator can be ignored, *ii*) near the resonance, the so-called *narrow width* approximation

$$\frac{1}{(s-m^2)^2 + m^2 \Gamma^2} \rightarrow \frac{\pi}{m \Gamma} \delta(s-m^2) \quad (2.14)$$

is valid. It is worth mentioning here that although the resonance occurs at a particular epoch $a = a_p$, it persists over a finite time. And *iii*) after the resonance, one can safely take $\Gamma_s = m_I = 0$ in the denominator.

By equating the second and third solutions of Eq. (2.13), one finds that the transition after the pole occurs at the scale factor a_t defined as

$$a_t \equiv a_I \left[\frac{32\pi^2}{3} \frac{2n-5}{n-2} \left(\frac{m_I}{\mu_h}\right)^2 \left(\frac{m_s}{2m_I}\right)^{\frac{2}{3} \frac{n-1}{n-2}} \right]^{\frac{2+n}{2(2n-5)}}. \quad (2.15)$$

Also, the end of reheating, defined as the onset of the radiation-dominated era, can be found by equating the third solution of Eq. (2.13) with Eq. (2.5), and the corresponding scale factor a_{rh} is

$$a_{\text{rh}} \simeq a_I \left(\frac{32\pi}{3} \frac{2n-5}{n} \frac{m_I^3 m_s^4}{H_I M_P^2 \mu_h^2 \mu_\phi^2} \right)^{\frac{2+n}{6(n-3)}}. \quad (2.16)$$

Finally, the SM temperature T can be extracted from the SM radiation energy density ρ_R by the fact that

$$\rho_R(T) = \frac{\pi^2}{30} g_\star(T) T^4, \quad (2.17)$$

⁶The recent BICEP/Keck bound on tensor-to-scalar ratio implies that $H_I \leq 2.0 \times 10^{-5} M_P$ [67]. This limit can also be used to derive an upper bound on the reheating temperature: $T_{\text{rh}} \lesssim 2.5 \times 10^{15}$ GeV under the assumption that the reheating is instantaneous [68].

where $g_*(T)$ corresponds to the number of relativistic degrees of freedom contributing to ρ_R . At $a = a_p$ the SM bath reaches a maximum temperature T_{\max} [69] given by

$$T_{\max} \simeq \left[\frac{45}{\pi g_*} \frac{n}{n-2} \left(\frac{m_s}{2m_I} \right)^{\frac{n+4}{n-2}} \frac{H_I^3 M_P^4 \mu_\phi^2}{m_I^2 m_s^3} \right]^{\frac{1}{4}}. \quad (2.18)$$

Furthermore, at the end of reheating, when $a = a_{\text{rh}}$, the SM temperature T_{rh} is

$$T_{\text{rh}} \simeq \left[\frac{90}{\pi^2 g_*} H_I^2 M_P^2 \left(\frac{3}{32\pi} \frac{n}{2n-5} \frac{H_I M_P^2 \mu_h^2 \mu_\phi^2}{m_I^3 m_s^4} \right)^{\frac{n}{n-3}} \right]^{\frac{1}{4}}. \quad (2.19)$$

In general, from Eq. (2.13) the scaling of the SM temperature can be extracted, and it is given by

$$T(a) \propto \begin{cases} a^{+\frac{3(2n-7)}{2(n+2)}} & \text{for } a_I \leq a \ll a_p, \\ a^{-1} & \text{for } a_p \leq a \ll a_t, \\ a^{-\frac{9}{2(n+2)}} & \text{for } a_t \leq a \ll a_{\text{rh}}. \end{cases} \quad (2.20)$$

We note that before the pole the SM temperature continuously increases with a slope $T(a) \propto a^{+\frac{3(2n-7)}{2(n+2)}}$, reaching the maximum $T = T_{\max}$ at $a = a_p$. Interestingly, near the resonance, the temperature decreases as $T(a) \propto a^{-1}$, independent of the value of n . In this case, the entropy injection and the Hubble expansion are counterbalanced, so that the SM radiation scales as free radiation. Well after the pole, the SM temperature continues to decrease, but more slowly, as $T(a) \propto a^{-\frac{9}{2(n+2)}}$ until the end of reheating at $a = a_{\text{rh}}$. After reheating, when the Universe becomes dominated by SM radiation, the SM entropy is conserved and therefore $T(a) \propto a^{-1}$. Before moving on, we clarify that in the present setup there are six free parameters that dictate the reheating dynamics, and can be conveniently chosen to be

$$n, m_I, H_I, m_s, \mu_h, \text{ and } \mu_\phi, \quad (2.21)$$

or

$$n, m_I, H_I, \frac{a_p}{a_I}, \frac{a_t}{a_I}, \text{ and } \frac{a_{\text{rh}}}{a_I}. \quad (2.22)$$

However, one can connect one set of parameters to the other using Eqs. (2.12), (2.15) and (2.16). For simplicity, in all numerical evaluations of this section, we will fix $m_I = 4 \times 10^{13}$ GeV and $H_I = 2 \times 10^{13}$ GeV, as inspired by α -attractor models [51, 52].

The fully numerical solution of the system of Boltzmann equations (2.2) and (2.3), using the varying inflaton mass in Eq. (2.7) together with the scattering rate in Eq. (2.10), is presented in Fig. 1 for $n = 4$, $m_s = 10^8$ GeV, $\mu_\phi = 10^{-2}$ GeV and $\mu_h = 10^6$ GeV. The left panel shows the energy densities for inflaton (blue) and SM radiation (black), while the right panel shows the evolution of the SM bath temperature T as a function of the scale factor. The red dotted vertical lines correspond to $a = a_p$, $a = a_t$, and $a = a_{\text{rh}}$, while the red dotted horizontal lines (in the right panel) correspond to $T = T_{\max}$, $T = T_t$, and $T = T_{\text{rh}}$. Furthermore, the three dotted black lines in the left panel show the analytical solutions in Eq. (2.13), which are in very good agreement with the numerical solution.

In Fig. 2 the dependence of the SM temperature on n is explored. We show the evolution of T as a function of the scale factor for $n = 4$ (solid line), $n = 6$ (dashed line), or $n = 8$

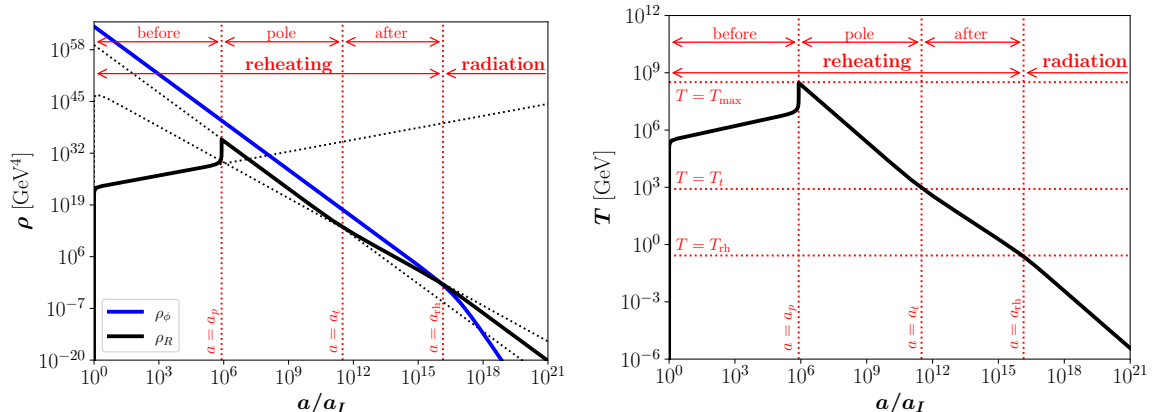


Figure 1. Bosonic reheating. Left: Evolution of the energy densities for the inflaton ρ_ϕ (solid blue) and the SM radiation ρ_R (solid black) as a function of the scale factor a . The three black dotted lines correspond to the analytical solutions in Eq. (2.13). Right: Evolution of SM temperature as a function of a . In both panels, $n = 4$, $m_s = 10^8$ GeV, $\mu_\phi = 10^{-2}$ GeV, $\mu_h = 10^6$ GeV, $m_I = 4 \times 10^{13}$ GeV and $H_I = 2 \times 10^{13}$ GeV were assumed. Here ‘before’, ‘pole’ and ‘after’ correspond to the epochs from the end of inflation until the pole ($a_I \leq a \leq a_p$), from the pole until the transition ($a_p \leq a \leq a_t$), and from the transition to the end of reheating ($a_t \leq a \leq a_{\text{rh}}$), respectively; cf. Eq. (2.13). The radiation-dominated era starts from $a = a_{\text{rh}}$.

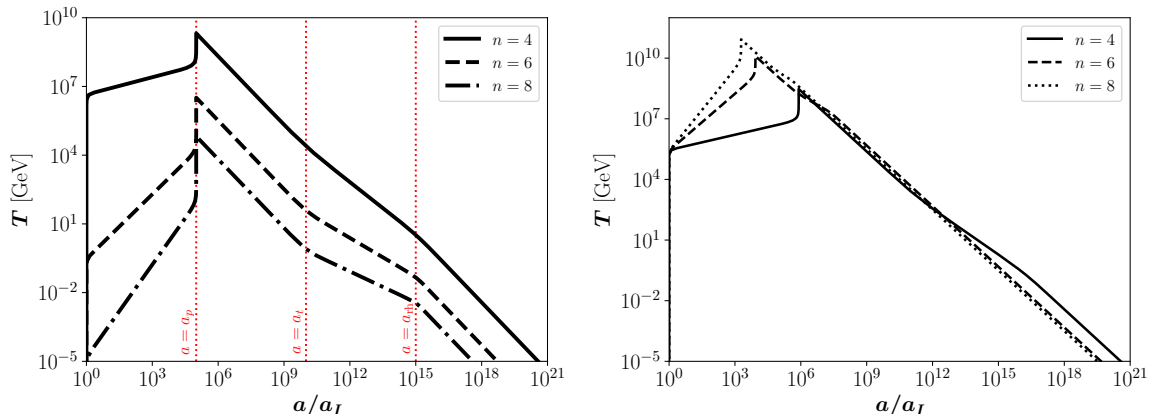


Figure 2. Bosonic reheating. Evolution of SM temperature T as a function of the scale factor a , for $n = 4$ (solid), 6 (dashed), or 8 (dashed-dotted). Left: $a_p/a_I = 10^5$, $a_t/a_I = 10^{10}$, $a_{\text{rh}}/a_I = 10^{15}$. Right: $m_s = 10^8$ GeV, $\mu_\phi = 10^{-2}$ GeV, and $\mu_h = 10^6$ GeV. In both panels, $m_I = 4 \times 10^{13}$ GeV and $H_I = 2 \times 10^{13}$ GeV.

(dashed-dotted line). In the left frame, we fix the scale factors $a_p/a_I = 10^5$, $a_t/a_I = 10^{10}$, $a_{\text{rh}}/a_I = 10^{15}$ (we therefore change the mediator mass and the couplings) so that the different slopes of the SM temperature are clear. Their behavior fits well with Eq. (2.20). In the right frame, we fix $m_s = 10^8$ GeV, $\mu_\phi = 10^{-2}$ GeV, and $\mu_h = 10^6$ GeV. In this panel, it is clear that, with an increase of n , the pole occurs earlier (as expected from Eq. (2.12)), and consequently T_{\max} is further enhanced due to the resonance.

In Fig. 3 we show the evolution of the inflaton (blue) and SM radiation (black) energy densities for $n = 4$ in the left panel, while the right panel shows the variation of the SM bath temperature T as a function of the scale factor. For a mediator that is always heavier

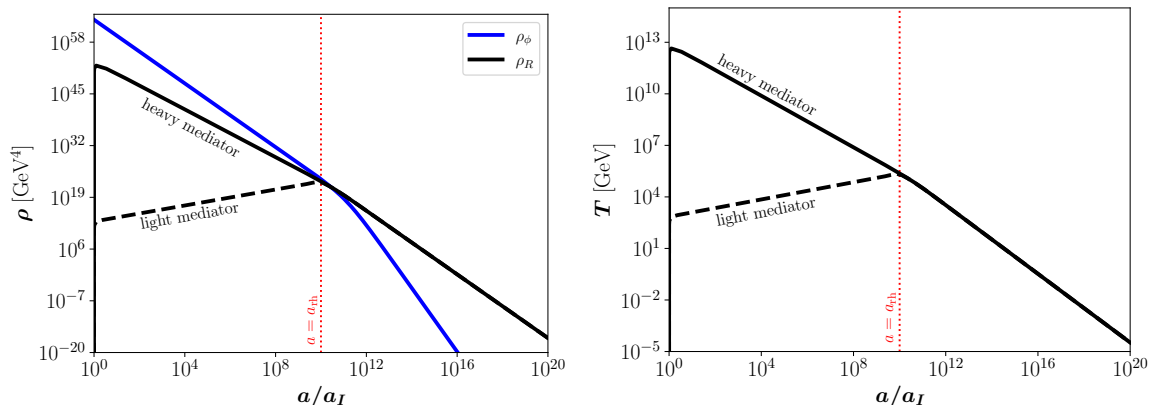


Figure 3. Bosonic reheating. Left: Evolution of the energy densities for inflaton ρ_ϕ (solid blue) and SM radiation ρ_R (black) as a function of the scale factor a . Right: Evolution of SM temperature as a function of a . In both panels, $n = 4$ and $a_{\text{rh}}/a_I = 10^{10}$. Solid black lines correspond to $m_s \gg m_I$ (heavy mediator), while dashed black lines correspond to $m_s \ll m_\phi(a_{\text{rh}})$ (light mediator). In both panels $m_I = 4 \times 10^{13}$ GeV and $H_I = 2 \times 10^{13}$ GeV.

than the inflaton (solid black lines), cf. $m_s \gg m_I$, no resonance develops during reheating. Essentially, if the mediator is heavy, it can be integrated out, and the reheating dynamics corresponds to the scenario in which the inflaton annihilates through a contact interaction [10, 11, 70]. It corresponds to the third case explored in Eqs. (2.13) and (2.20). Similarly, if the mediator is always lighter than the inflaton (dashed black lines), the resonance cannot develop either. However, it is interesting to note that in this case, with a light mediator, the temperature increases monotonically until the end of the reheating and consequently the reheating temperature $T_{\text{rh}} = T_{\text{max}}$. It corresponds to the first case in Eqs. (2.13) and (2.20). Note that the result presented in Fig. 1 corresponds to a transition between the limit cases of the heavy mediator and the light mediator.

2.2 Fermionic reheating

A successful reheating could also occur through inflaton annihilation into a pair of vector-like fermions ψ or e.g. right-handed neutrinos with mass m_ψ , mediated by S in the s channel: $\phi\phi \rightarrow S \rightarrow \psi\psi$. This can arise from the effective Lagrangian density

$$\mathcal{L} \supset \frac{1}{2} \tilde{\mu}_\phi \phi^2 S + y_f S \bar{\psi} \psi. \quad (2.23)$$

The corresponding annihilation rate reads

$$\Gamma_{\phi\phi \rightarrow \psi\psi} \simeq \frac{\rho_\phi}{m_\phi} \frac{1}{8\pi} \frac{\mu_\phi^2 y_f^2}{(4m_\phi^2 - m_s^2)^2 + m_s^2 \Gamma_s^2} \left(1 - \frac{m_\psi^2}{m_\phi^2}\right)^{\frac{3}{2}}, \quad (2.24)$$

and the total decay width for S

$$\Gamma_s = \frac{y_f^2 m_s}{8\pi} \left(1 - \frac{4m_f^2}{m_s^2}\right)^{\frac{3}{2}} \Theta(m_s - 2m_f) + \frac{1}{8\pi} \frac{\mu_\phi^2}{m_s} \sqrt{1 - \frac{4m_\phi^2}{m_s^2}} \Theta(m_s - 2m_\phi). \quad (2.25)$$

The system of Boltzmann equations (2.2) and (2.3) can be analytically solved following the same procedure as in the previous section. Consequently, the solution for the SM radiation energy is given by

$$\rho_R(a) \simeq \frac{9}{128\pi} \frac{H_I^3 M_P^4 y_f^2 \mu_\phi^2}{m_I^5} \times \begin{cases} \frac{n}{5n-11} \left(\frac{a}{a_I}\right)^{\frac{6(n-5)}{n+2}} \left[1 - \left(\frac{a_I}{a}\right)^{\frac{2(5n-11)}{2+n}}\right] & \text{for } a_I \leq a < a_p, \\ \frac{n}{n-1} \left(\frac{2m_I}{m_s}\right)^4 \left(\frac{a_I}{a}\right)^4 \left[1 - \left(\frac{a_I}{a}\right)^{\frac{2(n-1)}{n+2}}\right] & \text{for } a_p < a, \end{cases} \quad (2.26)$$

where a_p is again the scale factor where the pole is reached (i.e. $m_\phi(a_p) = m_s/2$), given in Eq. (2.12), and corresponds to a maximal temperature of the SM plasma

$$T_{\max} \simeq \left[\frac{135}{64\pi^3 g_\star} \frac{n}{n-1} \frac{H_I^3 M_P^4 y_f^2 \mu_\phi^2}{m_I^5} \left(\frac{2m_I}{m_s}\right)^{\frac{8(n-4)}{3(n-2)}} \right]^{\frac{1}{4}}. \quad (2.27)$$

The analytical solution for the SM energy density in the fermionic case in Eq. (2.26) can be divided into two cases (instead of three as in the bosonic case; cf. Eq. (2.13)), as the scaling of ρ_R during and after the pole is the same, $\rho_R(a) \propto a^{-4}$.

The end of reheating, defined as the moment at which the Universe transitions to a radiation-dominated epoch, happens at a scale factor

$$a_{\text{rh}} \simeq a_I \left(\frac{8\pi}{3} \frac{n-1}{n} \frac{m_I m_s^4}{H_I M_P^2 y_f^2 \mu_\phi^2} \right)^{\frac{n+2}{2(n-4)}}, \quad (2.28)$$

corresponding to the temperature

$$T_{\text{rh}} \simeq \left[\frac{90}{\pi^2 g_\star} H_I^2 M_P^2 \left(\frac{3}{8\pi} \frac{n}{n-1} \frac{H_I M_P^2 y_f^2 \mu_\phi^2}{m_I m_s^4} \right)^{\frac{3n}{n-4}} \right]^{\frac{1}{4}}. \quad (2.29)$$

Finally, we observe from Eq. (2.26) that the SM temperature scales as

$$T(a) \propto \begin{cases} a^{\frac{3(n-5)}{2(n+2)}} & \text{for } a_I < a < a_p, \\ a^{-1} & \text{for } a_p < a. \end{cases} \quad (2.30)$$

The fully numerical solution of the system of Boltzmann equations for the fermionic case is presented in Fig. 4 for $n = 6$, $m_s = 10^8$ GeV, $\mu_\phi = 10^{-2}$ GeV and $y_f = 10^{-2}$. The left panel shows the energy densities for the inflaton (blue) and SM radiation (black), while the right panel shows the evolution of the SM bath temperature T as a function of the scale factor. The red dotted vertical lines correspond to $a = a_p$ and $a = a_{\text{rh}}$, while the red dotted horizontal lines (in the right panel) correspond to $T = T_{\max}$ and $T = T_{\text{rh}}$. Furthermore, the two dotted black lines in the left panel show the analytical solutions in Eq. (2.26), which is in very good agreement with the numerical solution.

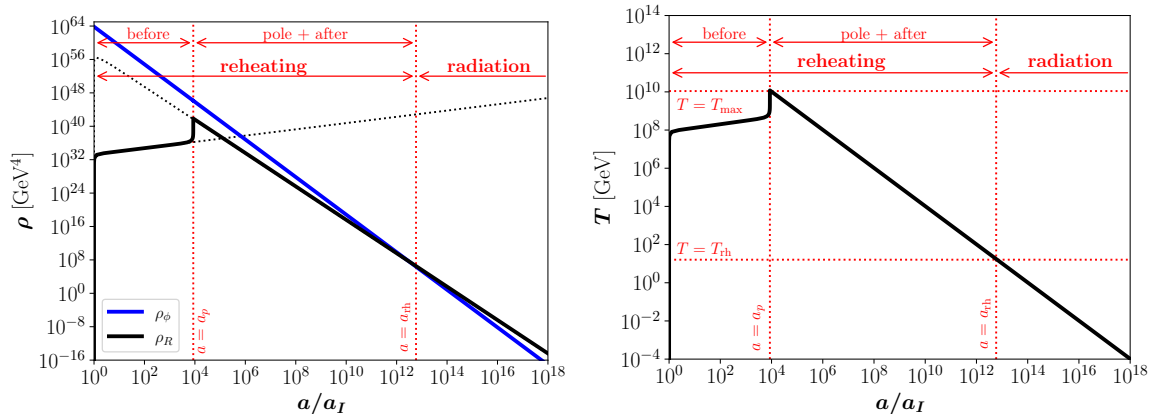


Figure 4. Fermionic reheating. Left: Evolution of the energy densities for the inflaton ρ_ϕ (solid blue) and the SM radiation ρ_R (solid black) as a function of the scale factor a . The two black dotted lines correspond to the analytical solutions in Eq. (2.26). Right: Evolution of the SM temperature as a function of a . In both panels, $n = 6$, $m_s = 10^8$ GeV, $\mu_\phi = 10^{-2}$ GeV, $y_f = 10^{-3}$, $m_I = 4 \times 10^{13}$ GeV and $H_I = 2 \times 10^{13}$ GeV were assumed.

3 Dark matter freeze-in during resonant reheating

The DM number can then be tracked by solving the Boltzmann equation for its number density n_{dm}

$$\frac{dn_{\text{dm}}}{dt} + 3Hn_{\text{dm}} = \gamma, \quad (3.1)$$

where γ is the DM production reaction rate density. As the SM entropy is not conserved during reheating due to the annihilation of the inflaton in SM particles, it is convenient to introduce a comoving number density $N_{\text{dm}} \equiv n_{\text{dm}} a^3$, and therefore Eq. (3.1) can be rewritten as

$$\frac{dN_{\text{dm}}}{da} = \frac{a^2 \gamma}{H}, \quad (3.2)$$

which has to be numerically solved together with Eqs. (2.2) and (2.3), taking the initial condition $N_{\text{dm}}(a_I) = 0$. To fit the whole observed DM relic density, it is required that

$$Y_0 m_{\text{dm}} = \Omega h^2 \frac{1}{s_0} \frac{\rho_c}{h^2} \simeq 4.3 \times 10^{-10} \text{ GeV}, \quad (3.3)$$

where $Y_0 \equiv Y(T_0)$ and $Y(T) \equiv n_{\text{dm}}(T)/s(T)$, with s being the SM entropy density defined by

$$s(T) = \frac{2\pi^2}{45} g_{\star s}(T) T^3, \quad (3.4)$$

and $g_{\star s}(T)$ being the number of relativistic degrees of freedom contributing to the SM entropy. Furthermore, $\rho_c \simeq 1.05 \times 10^{-5} h^2 \text{ GeV/cm}^3$ is the critical energy density, $s_0 \simeq 2.69 \times 10^3 \text{ cm}^{-3}$ the present entropy density [71], and $\Omega h^2 \simeq 0.12$ the observed abundance of DM relics [72].

In the early Universe, DM can be produced from 2-to-2 scattering of SM thermal bath particles or inflatons, mediated by S .⁷ Additionally, it can also be mediated by the exchange of gravitons. In the following subsections, the DM production will be discussed in detail.

⁷We note that the inflaton annihilation into a pair of S particles than subsequently decay into DM states is also viable, however it is subdominant in our scenario as discussed in Appendix A.

3.1 From the thermal bath

In this section, we investigate the impact of resonant reheating, presented in the previous section, on dark matter (DM) yield. We consider the simplest scenario, where the DM is a real singlet scalar φ of mass m_{dm} , with an interaction Lagrangian that reads

$$\mathcal{L}_{\text{dm}} \supset \frac{1}{2} m_{\text{dm}}^2 \varphi^2 + \frac{1}{2} \mu_{\text{dm}} S \varphi^2, \quad (3.5)$$

assuming that the only mediator between the SM, the inflaton and DM is S , and again ignoring quartic couplings. Here, we consider any explicit coupling between the DM and the inflaton, and quartic interactions between the mediator S or the SM Higgs doublet and the DM are absent by construction. We again remain agnostic about the UV completion of such scenarios and focus mainly on the aftermath of resonant reheating on DM production. The only interaction that the DM can have with the visible sector is mediated by S , as can be seen in Eq. (3.5). Therefore, DM can be produced in the early Universe from the bath via the scattering of SM Higgs, mediated by S . This process can occur during (inflaton domination) and after (radiation domination) reheating; however, the effect of resonant reheating can only be seen in the former scenario. Now, if the interaction strength between the DM and the visible sector is sufficiently weak to ensure that the DM never thermalizes with the radiation bath, then the production of DM takes place through the freeze-in paradigm. This is the approach that follows.

As mentioned above, the DM yield is governed by the 2-to-2 scattering of the bath particles (Higgs), mediated by the scalar S . The corresponding cross-section for this process reads

$$\sigma(s)_{hh \rightarrow \varphi\varphi} \simeq \frac{1}{8\pi s} \frac{(\mu_{\text{dm}} \mu_h)^2}{(s - m_s^2)^2 + \Gamma_s^2 m_s^2} \sqrt{1 - \frac{4m_{\text{dm}}^2}{s}}, \quad (3.6)$$

where Γ_s is given by (following Eqs. (2.9) and (3.5))

$$\Gamma_s = \frac{1}{8\pi} \frac{\mu_h^2}{m_s} \sqrt{1 - \frac{4m_h^2}{m_s^2}} + \frac{1}{8\pi} \frac{\mu_\phi^2}{m_s} \sqrt{1 - \frac{4m_\phi^2}{m_s^2}} + \frac{1}{8\pi} \frac{\mu_{\text{dm}}^2}{m_s} \sqrt{1 - \frac{4m_{\text{dm}}^2}{m_s^2}}, \quad (3.7)$$

where the last term corresponds to S decay into a pair of DM particles. In the left panel of Fig. 5 the production cross section is shown as a function of the center-of-mass energy s , for $m_s = 10^8$ GeV, $m_{\text{dm}} = 10^6$ GeV, $\mu_h = 10^6$ GeV and $\mu_\phi = 10^{-2}$ GeV. The resonance at $\sqrt{s} \simeq m_s$ is clearly visible as a peak in the cross section.

One can further define the interaction rate density as

$$\gamma = \gamma_{hh \rightarrow \varphi\varphi} = \frac{T}{2\pi^4} \int_{4m_{\text{dm}}^2}^{\infty} ds s^{3/2} \sigma(s)_{hh \rightarrow \varphi\varphi} K_1\left(\frac{\sqrt{s}}{T}\right), \quad (3.8)$$

which takes the approximate form for $m_{\text{dm}} \ll m_s$

$$\gamma_{hh \rightarrow \varphi\varphi} \simeq \frac{T}{2\pi^4} \frac{1}{8\pi} \frac{(\mu_{\text{dm}} \mu_h)^2}{1} \times \begin{cases} \frac{4m_{\text{dm}}^2 T}{m_s^4} K_1^2\left(\frac{m_{\text{dm}}}{T}\right) & \text{for } T \ll \frac{m_s}{2}, \\ \frac{\pi}{\Gamma_s} K_1\left(\frac{m_s}{T}\right) \sqrt{1 - \frac{4m_{\text{dm}}^2}{m_s^2}} & \text{for } T \gg \frac{m_s}{2}, \end{cases} \quad (3.9)$$

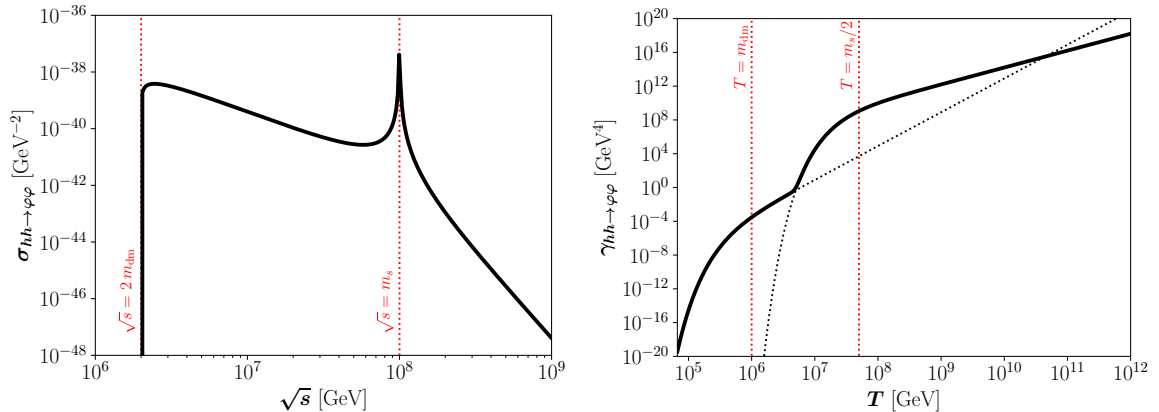


Figure 5. Cross section (left) and production rate density (right), for $m_s = 10^8$ GeV, $m_{\text{dm}} = 10^6$ GeV, $\mu_h = 10^6$ GeV and $\mu_\phi = 10^{-2}$ GeV. The black dotted lines in the right panel correspond to the analytical solution in Eq. (3.9).

or in the opposite case where $m_s \ll m_{\text{dm}}$

$$\gamma_{hh \rightarrow \varphi\varphi} \simeq \frac{T}{2\pi^4} \frac{1}{8\pi} \frac{(\mu_{\text{dm}} \mu_h)^2}{1} \times \begin{cases} \frac{\pi T^2}{8 m_{\text{dm}}^3} e^{-\frac{2m_{\text{dm}}}{T}} & \text{for } T \ll m_{\text{dm}}, \\ \frac{T}{6 m_{\text{dm}}^2} & \text{for } T \gg m_{\text{dm}}, \end{cases} \quad (3.10)$$

with $K_1(x)$ being the modified Bessel function of the first kind. Here, we have ignored the masses of the initial states, a reasonable approximation during reheating, which occurs at a very high temperature, much before the electroweak symmetry is broken. The right panel of Fig. 5 shows the production rate density as a function of temperature T , for $m_s = 10^8$ GeV, $m_{\text{dm}} = 10^6$ GeV, $\mu_h = 10^6$ GeV and $\mu_\phi = 10^{-2}$ GeV. The black dotted lines correspond to the analytical solution in Eq. (3.9), in good agreement with the fully numerical solution. Interestingly, the sharp peak in the cross section appears as a smooth bump in the rate density.

In Fig. 6 examples of the evolution of the comoving DM abundance as a function of the scale factor a are shown for $n = 4$, $a_p/a_I = 10^5$, $a_t/a_I = 10^{10}$, $a_{\text{rh}}/a_I = 10^{15}$, and $m_{\text{dm}} = 10^{-4}$ GeV and $\mu_{\text{dm}} = 2 \times 10^{-3}$ GeV (top left), $m_{\text{dm}} = 10^0$ GeV and $\mu_{\text{dm}} = 5 \times 10^{-2}$ GeV (top right), or $m_{\text{dm}} = 10^4$ GeV and $\mu_{\text{dm}} = 3 \times 10^{-1}$ GeV (bottom). In this section, we take $m_I = 10^{12}$ GeV and $H_I = 5 \times 10^8$ GeV, to avoid gravitational overproduction, as will be seen in Section 3.3. The vertical red dotted lines correspond to the scale factors for which $T = T_{\text{max}}$, $T = T_t$, or $T = T_{\text{rh}}$, while the dashed red lines correspond to $T = m_{\text{dm}}$. All these benchmark points fit well the observed relic abundance, represented by a horizontal blue band. The detailed evolution of these benchmark points will be described in the following.

For light DM particles, with masses below T_{rh} (and m_s), the heavy mediator S can be safely integrated out so that the cross section in Eq. (3.6) effectively scales as $\sigma(s) \propto \mu_h^2 \mu_{\text{dm}}^2 / (s m_s^4)$, and therefore the interaction rate density $\gamma(T) \propto \mu_h^2 \mu_{\text{dm}}^2 T^4 / m_s^4$; cf. the first line of Eq. (3.9) in the limit $m_{\text{dm}} \ll T$. In this case, DM is a standard IR FIMP, produced at low temperatures, mainly when $T \sim m_{\text{dm}}$, as shown in the upper left panel of Fig. 6. The

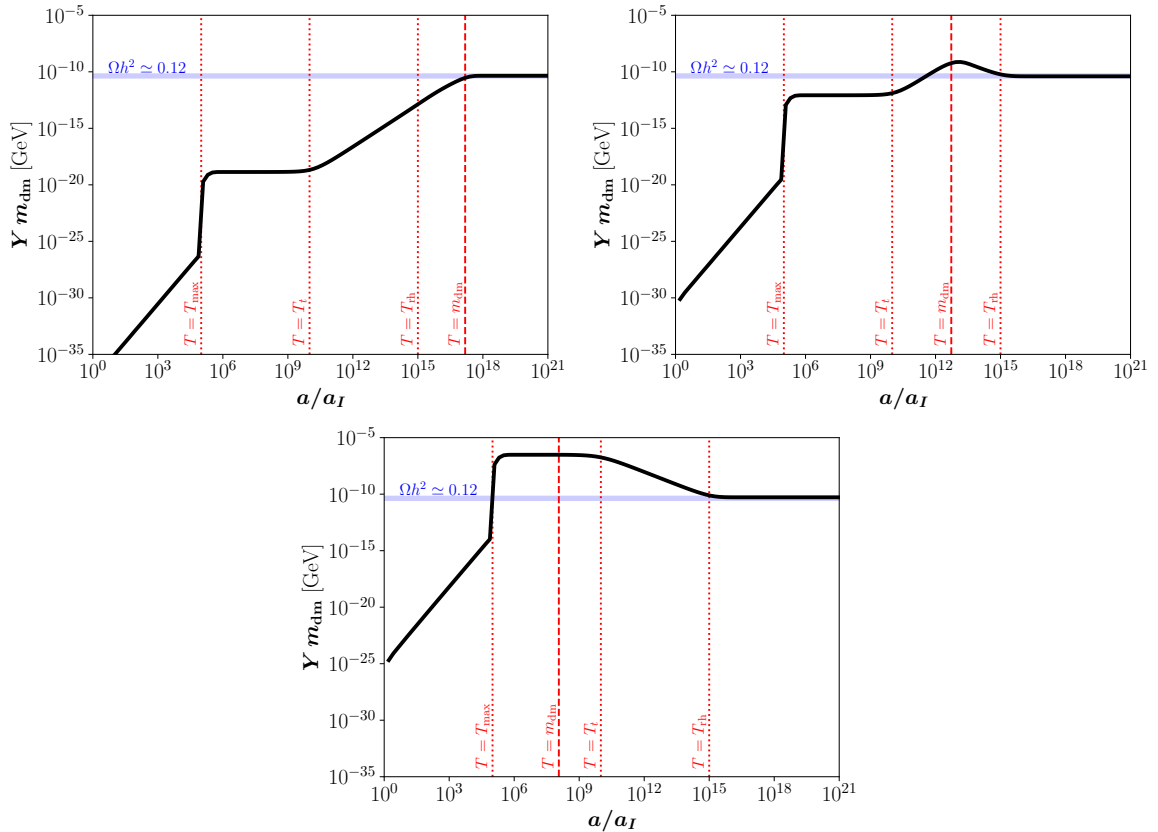


Figure 6. DM production from the thermal bath. Evolution of the comoving abundance of DM as a function of the scale factor a , for $n = 4$, $a_p/a_I = 10^5$, $a_t/a_I = 10^{10}$, $a_{rh}/a_I = 10^{15}$, and $m_{\text{dm}} = 10^{-4}$ GeV and $\mu_{\text{dm}} = 2 \times 10^{-3}$ GeV (top left), $m_{\text{dm}} = 10^0$ GeV and $\mu_{\text{dm}} = 5 \times 10^{-2}$ GeV (top right), or $m_{\text{dm}} = 10^4$ GeV and $\mu_{\text{dm}} = 3 \times 10^{-1}$ GeV (bottom). In all panels $m_I = 10^{12}$ GeV and $H_I = 5 \times 10^8$ GeV. The horizontal blue band corresponds to the abundance of DM measured by Planck.

approximate analytical solution of Eq. (3.2) reads

$$Y_0 \simeq \frac{135}{64\pi^7 g_{\star s}} \sqrt{\frac{10}{g_{\star}}} \frac{\mu_{\text{dm}}^2 \mu_h^2 M_P}{m_{\text{dm}} m_s^4} \quad (3.11)$$

and, as expected, is independent on the reheating dynamics. Interestingly, to fit the total observed relic abundance of DM, cf. Eq. (3.3), the required inflaton coupling to DM is independent of the mass of DM. This can be seen in Fig. 7, where the thick black line shows the parameter space in the plane $[m_{\text{dm}}, \mu_{\text{dm}}]$ that fits the entire observed abundance of DM.

The second case corresponds to intermediate masses of DM in the range $T_{\text{rh}} \lesssim m_{\text{dm}} \lesssim T_t$. This case resembles the previous one, with the difference that in the range $a_t < a < a_{\text{rh}}$ the temperature scales as $T(a) \propto a^{-\frac{9}{2(n+2)}}$, cf. Eq. (2.20). DM is constantly produced in the range $T_t \gtrsim T \gtrsim m_{\text{dm}}$, and stops when the temperature is of the order of its mass, due to kinematical reasons. After production stops, during the range $m_{\text{dm}} \gtrsim T \gtrsim T_{\text{rh}}$, the injection of entropy due to the decay of the inflaton into the SM states dilutes the abundance of DM.

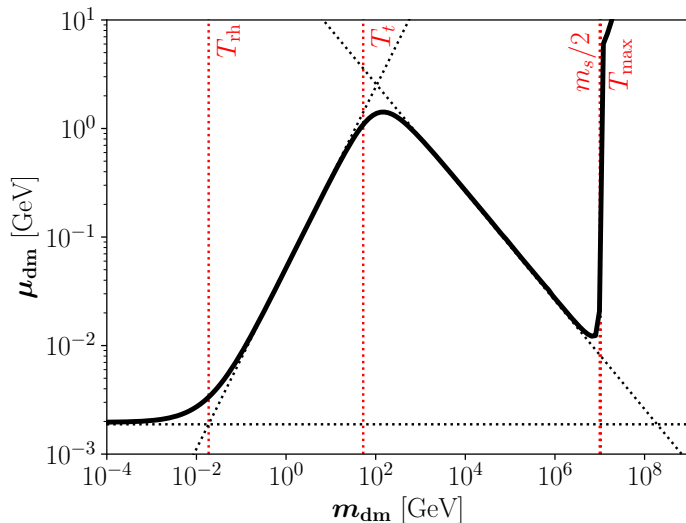


Figure 7. DM production from the thermal bath. Parameter space that fits the entire observed DM abundance (black thick line), for $n = 4$, $a_p/a_I = 10^5$, $a_t/a_I = 10^{10}$, $a_{rh}/a_I = 10^{15}$, $m_I = 10^{12}$ GeV and $H_I = 5 \times 10^8$ GeV. The black dotted lines correspond to the analytical solutions described in the text.

In this regime, the approximate analytical solution of Eq. (3.2) reads

$$Y_0 \simeq \frac{135}{8\pi^8 g_\star} \sqrt{\frac{10}{g_\star}} \frac{\Gamma\left[\frac{6(n-2)}{n+2}\right]}{\Gamma\left[\frac{7n-10}{n+2}\right]} \frac{\mu_{\text{dm}}^2 \mu_h^2 M_P}{m_s^4 T_{\text{rh}}} \left(\frac{T_{\text{rh}}}{m_{\text{dm}}}\right)^{\frac{4(n-2)}{3}}, \quad (3.12)$$

showing a strong dependence on the reheating dynamics, as expected in the case of a UV FIMP. To fit the observed DM abundance, the inflaton coupling to DM has to scale as

$$\mu_{\text{dm}} \propto m_{\text{dm}}^{\frac{4n-11}{6}}, \quad (3.13)$$

as shown in Fig. 7 in the range $T_{\text{rh}} \lesssim m_{\text{dm}} \lesssim T_t$.

The third case corresponds to heavy DM, with mass in the range $T_t \lesssim m_{\text{dm}} \lesssim m_s$. The interaction rate density can be approximated as $\gamma(T) \propto \mu_{\text{dm}}^2 m_s^2 (T/m_s)^{\frac{3}{2}} e^{-\frac{m_s}{T}}$, cf. the second line of Eq. (3.9) in the limit $T \ll m_s$. Several comments are in order: *i*) the exponential factor stops DM production for temperatures below the mass of S , *ii*) since in this period the SM radiation behaves as free radiation (cf. Eq. (2.20)), there is effectively no entropy dilution and, therefore, the DM yield is constant, and *iii*) there is, however, a dilution of the abundance of DM in the era $T_t > T > T_{\text{rh}}$. An example of the evolution of the DM yield for this case can be seen in the lower panel of Fig. 6. An approximate analytical solution of Eq. (3.2) is

$$Y_0 \simeq \frac{135}{4\sqrt{2} \pi^{\frac{11}{2}} g_{\star s}} \sqrt{\frac{10}{g_\star}} \frac{\mu_{\text{dm}}^2 m_s^2 M_P}{T_{\text{rh}}^5} \left(\frac{a_p}{a_{\text{rh}}} \frac{T_{\text{max}}}{m_s}\right)^{\frac{6(n+1)}{n+2}}. \quad (3.14)$$

We note that as the rate density is independent of the DM mass, it is required that

$$\mu_{\text{dm}} \propto m_{\text{dm}}^{-1/2}, \quad (3.15)$$

to fit the observed DM abundance, as shown in Fig. 7

Finally, we also note that when $m_{\text{dm}} > m_s/2$, the DM production becomes Boltzmann suppressed, requiring a sudden increase of μ_{dm} , as shown in Fig. 7. Overall, it is interesting to see that this behavior significantly differs from the freeze-in during standard reheating scenarios; see, e.g. Refs. [73–76].

3.2 From inflaton annihilations

In our setup, another possible DM production channel occurs through the inflaton annihilation via an s -channel exchange of the mediator S , i.e. $\phi\phi \rightarrow S \rightarrow \varphi\varphi$. The production rate density is given by⁸

$$\gamma = \gamma_{\phi\phi \rightarrow \varphi\varphi} = + \frac{2n}{n+2} \frac{\Gamma_{\phi\phi \rightarrow \varphi\varphi} \rho_\phi}{m_\phi}, \quad (3.16)$$

with

$$\Gamma_{\phi\phi \rightarrow \varphi\varphi} \simeq \frac{\rho_\phi}{m_\phi} \frac{\mu_\phi^2 \mu_{\text{dm}}^2}{32\pi m_\phi^2 \left[(4m_\phi^2 - m_s^2)^2 + \Gamma_s^2 m_s^2 \right]} \sqrt{1 - \frac{m_{\text{dm}}^2}{m_\phi^2}} \Theta(m_\phi - m_{\text{dm}}). \quad (3.17)$$

Examples of the evolution of the comoving DM abundance N (left) and Y (right) as a function of the scale factor a are shown in Fig. 8 for $n = 4$, $a_p/a_I = 10^5$, $a_t/a_I = 10^{10}$, $a_{\text{rh}}/a_I = 10^{15}$, and $m_{\text{dm}} = 10^{-5}$ GeV and $\mu_{\text{dm}} = 2 \times 10^2$ GeV (top), $m_{\text{dm}} = 10^{-1}$ GeV and $\mu_{\text{dm}} = 25$ GeV (second from top), $m_{\text{dm}} = 10^4$ GeV and $\mu_{\text{dm}} = 2$ GeV (third from top), or $m_{\text{dm}} = 10^9$ GeV and $\mu_{\text{dm}} = 7 \times 10^5$ GeV (bottom). The vertical red dotted lines correspond to the scale factors for which $T = T_{\text{max}}$, $T = T_t$, or $T = T_{\text{rh}}$, while the dashed red lines correspond to $m_\phi = m_{\text{dm}}$. All four benchmark points fit well the observed relic abundance, represented by a horizontal blue band (right). The detailed evolution of these four benchmark points will be described in the following.

In this scenario, the abundance of DM can be analytically estimated in different regimes, depending on its mass with respect to the varying inflaton mass. Light DM, with mass $m_{\text{dm}} < m_\phi(T_{\text{rh}})$, is produced mainly at $T \simeq T_{\text{rh}}$ (top panel of Fig. 8). This corresponds to a UV freeze-in during radiation dominance, with an interaction driven by a heavy mediator. An approximate analytical solution of Eq. (3.2) is

$$Y_0 \simeq \frac{135}{64\pi^3 g_{\star s}} \frac{n}{n-3} \frac{\mu_{\text{dm}}^2 \mu_\phi^2 H_I^3 M_P^4}{m_I^4 m_s^4 T_{\text{rh}}^3} \left(\frac{a_I}{a_{\text{rh}}} \right)^{\frac{3(8-n)}{2+n}}. \quad (3.18)$$

To fit the total observed relic abundance of DM, cf. Eq. (3.3), the required inflaton coupling to DM has to scale as

$$\mu_{\text{dm}} \propto m_{\text{dm}}^{-\frac{1}{2}}, \quad (3.19)$$

as shown in Fig. 9 in the plane $[m_{\text{dm}}, \mu_{\text{dm}}]$.

The second case corresponds to DM with mass $m_\phi(T_{\text{rh}}) < m_{\text{dm}} < m_\phi(T_t)$. The bulk of DM density starts to be produced at $T = T_t$ and stops when $m_\phi = m_{\text{dm}}$, due to kinematics, at a scale factor a_{dm} given by

$$a_{\text{dm}} \equiv a_I \left(\frac{m_I}{m_{\text{dm}}} \right)^{\frac{n+2}{3(n-2)}}, \quad (3.20)$$

⁸We note that a factor $1 + \omega \equiv \frac{2n}{2+n}$ shall be included on the right handed side of the Boltzmann equation for the DM number density.

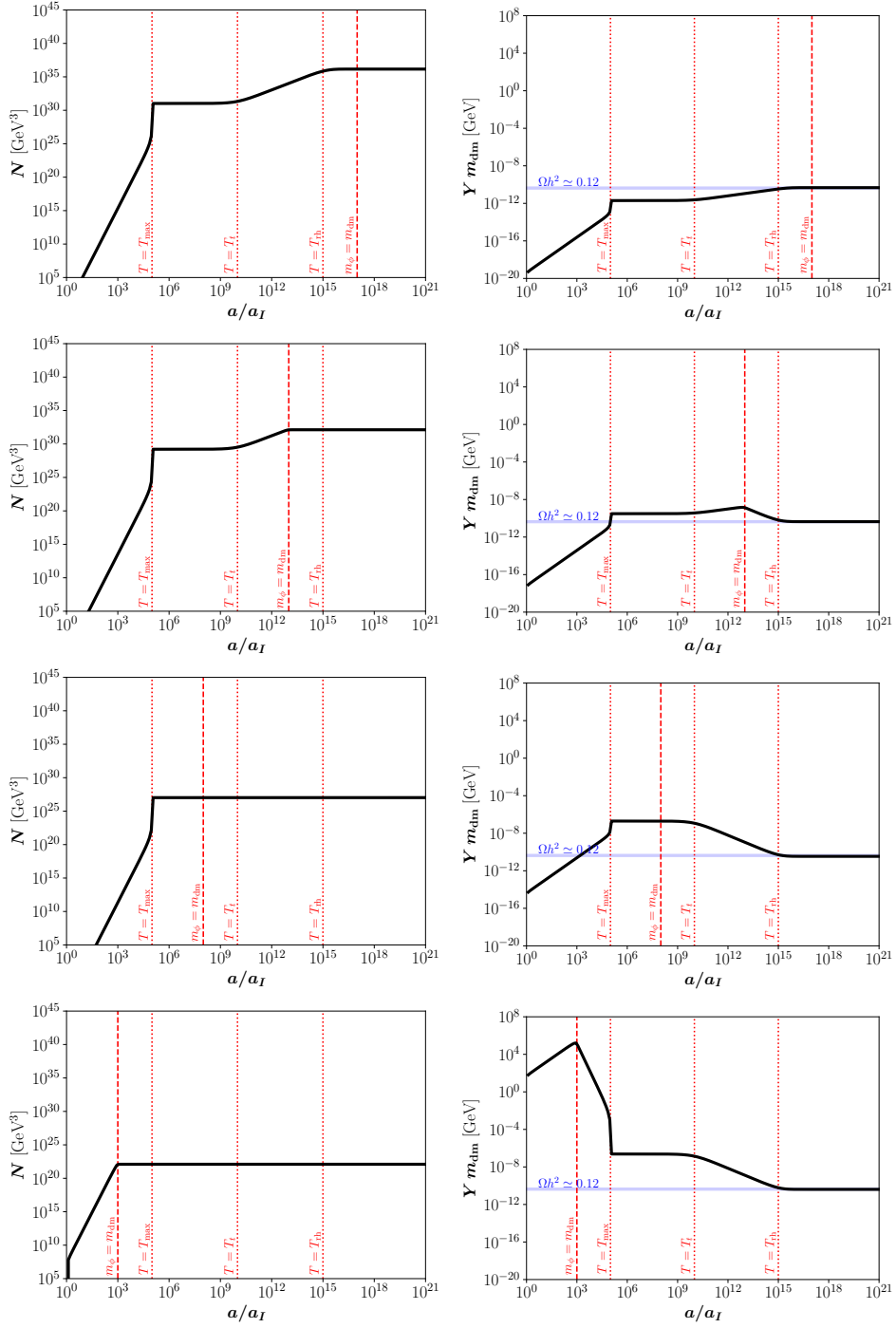


Figure 8. DM production from inflaton annihilations. Evolution of the comoving DM abundance N (left) and Y (right) as a function of the scale factor a , for $n = 4$, $a_p/a_I = 10^5$, $a_t/a_I = 10^{10}$, $a_{\text{rh}}/a_I = 10^{15}$, and $m_{\text{dm}} = 10^{-5}$ GeV and $\mu_{\text{dm}} = 2 \times 10^2$ GeV (top), $m_{\text{dm}} = 10^{-1}$ GeV and $\mu_{\text{dm}} = 25$ GeV (second from top), $m_{\text{dm}} = 10^4$ GeV and $\mu_{\text{dm}} = 2$ GeV (third from top), or $m_{\text{dm}} = 10^9$ GeV and $\mu_{\text{dm}} = 7 \times 10^5$ GeV (bottom). In all panels $m_I = 10^{12}$ GeV and $H_I = 5 \times 10^8$ GeV. The horizontal blue band corresponds to the abundance of DM measured by Planck.

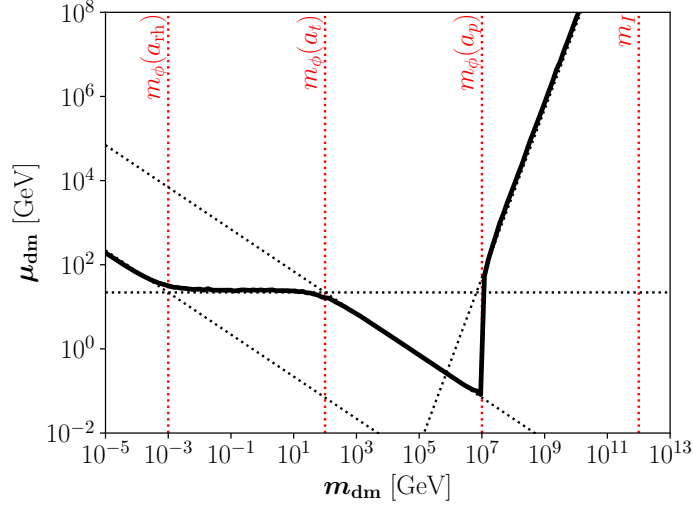


Figure 9. DM production from inflaton annihilations. Parameter space that fits the entire observed DM abundance (black thick line), for $n = 4$, $a_p/a_I = 10^5$, $a_t/a_I = 10^{10}$, $a_{\text{rh}}/a_I = 10^{15}$, $m_I = 10^{12}$ GeV and $H_I = 5 \times 10^8$ GeV. The black dotted lines correspond to the analytical solutions described in the text.

as shown in the second from top panel in Fig. 8. Between $m_\phi = m_{\text{dm}}$ and $T = T_{\text{rh}}$ large entropy injection dilutes the DM abundance; the final DM yield is estimated as

$$Y_0 \simeq \frac{135}{64\pi^3 g_{\star s}} \frac{n}{n-3} \frac{\mu_\phi^2 \mu_{\text{dm}}^2 M_P^4 H_I^3}{m_I^4 m_s^4 T_{\text{rh}}^3} \left(\frac{a_I}{a_{\text{rh}}}\right)^3 \left(\frac{m_I}{m_{\text{dm}}}\right)^{\frac{2(n-3)}{n-2}}, \quad (3.21)$$

which implies that, to fit the observed DM abundance, the inflaton coupling to DM has to scale as

$$\mu_{\text{dm}} \propto m_{\text{dm}}^{\frac{n-4}{2(n-2)}}. \quad (3.22)$$

For the case $n = 4$, μ_{dm} is independent of the DM mass, as shown in Fig. 9.

The third case corresponds to DM with mass $m_\phi(T_t) < m_{\text{dm}} < m_\phi(T_p) = 2m_s$ produced mainly at $m_{\text{dm}} = 2m_s$, when $T = T_{\text{max}}$, which is a clear example of a UV freeze-in during reheating; cf. the third panel from the top in Fig. 8. Here, the interaction rate density in Eq. (3.17) is dominated by the pole. The DM abundance is then diluted during the period $T_t > T > T_{\text{rh}}$, the final yield being

$$Y_0 \simeq \frac{135}{16\pi^2 g_{\star s}} \frac{n}{n-2} \frac{\mu_\phi^2 \mu_{\text{dm}}^2 M_P^4 H_I^3}{m_I^2 m_s^5 T_{\text{rh}}^3 \Gamma_s} \left(\frac{a_I}{a_{\text{rh}}}\right)^3 \left(\frac{m_s}{2m_I}\right)^{\frac{2}{n-2}}, \quad (3.23)$$

implying that

$$\mu_{\text{dm}} \propto m_{\text{dm}}^{-\frac{1}{2}} \quad (3.24)$$

to fit the observed DM abundance, as seen in Fig. 9.

Finally, the fourth case corresponds to the heavy DM with mass $2m_s < m_{\text{dm}} < m_I$, which is produced mainly around $m_{\text{dm}} = m_\phi$, when the scale factor is given by Eq. (3.20). The abundance of DM suffers two periods of dilution, from $m_\phi = m_{\text{dm}}$ to $T = T_{\text{max}}$, and

then during the interval $T_t > T > T_{\text{rh}}$; see the lower panel of Fig. 8. The final DM yield is therefore

$$Y_0 \simeq \frac{135}{1024\pi^3 g_{*s}} \frac{n}{3n-7} \left(\frac{a_I}{a_{\text{rh}}}\right)^3 \frac{H_I^3 M_P^4 \mu_{\text{dm}}^2 \mu_\phi^2}{m_I^8 T_{\text{rh}}^3} \left(\frac{m_I}{m_{\text{dm}}}\right)^{\frac{2(3n-7)}{n-2}}, \quad (3.25)$$

implying that

$$\mu_{\text{dm}} \propto m_{\text{dm}}^{\frac{5n-12}{2(n-2)}} \quad (3.26)$$

to fit the observed DM abundance, as seen in Fig. 9. We note that DM particles heavier than the inflaton ($m_{\text{dm}} > m_I$) are kinematically forbidden in this channel.

3.3 Gravitational production

Gravity is the only interaction that is guaranteed to mediate between the DM and the visible sector, and therefore it has to be taken into account. DM can indeed be produced by the scattering of inflatons or SM particles, mediated by the s -channel exchange of gravitons. Below we briefly discuss the DM gravitational production.

From the thermal bath

DM is unavoidably produced from the UV freeze-in mechanism via 2-to-2 annihilation of the SM particles mediated by s -channel exchange of gravitons [77–79]. The interaction rate density for such a process reads

$$\gamma = \alpha \frac{T^8}{M_P^4} \quad (3.27)$$

with $\alpha \simeq 1.9 \times 10^{-4}$ for real scalar DM [17, 68, 80]. In the cosmological scenario presented here, DM is produced mainly at $T = T_{\text{max}}$ and then diluted during the period $T_t > T > T_{\text{rh}}$. An approximate analytical solution of Eq. (3.2) is

$$Y_0 \simeq \frac{45\alpha}{4\pi^2 g_{*s}} \frac{n+2}{n+5} \frac{T_{\text{max}}^8}{H_I M_P^4 T_{\text{rh}}^3} \left(\frac{a_I}{a_{\text{rh}}}\right)^3 \left(\frac{a_p}{a_I}\right)^{\frac{6(n+1)}{n+2}}. \quad (3.28)$$

From inflaton annihilations

During reheating, the whole observed DM abundance can be generated via 2-to-2 annihilations of inflatons, mediated by the s -channel exchange of gravitons. The interaction rate density for DM production reads [81–83]

$$\gamma = \frac{2n}{n+2} \frac{\rho_\phi^2}{256\pi M_P^4} f\left(\frac{m_{\text{dm}}}{m_\phi}\right), \quad (3.29)$$

with

$$f(x) = (x^2 + 2)^2 \sqrt{1 - x^2} \quad (3.30)$$

for real scalar DM [68]. The bulk of the DM relic density is promptly produced at the beginning of the reheating era ($a = a_I$), and suffers two periods of dilution: $a_I > a > a_p$ and $a_t > a > a_{\text{rh}}$. The final DM yield can be analytically estimated as

$$Y_0 \simeq \frac{135}{256\pi^3 g_{*s}} \frac{2n}{n-1} \left(\frac{H_I}{T_{\text{rh}}}\right)^3 \left(\frac{a_I}{a_{\text{rh}}}\right)^3 \left[1 - \left(\frac{a_I}{a_{\text{rh}}}\right)^{\frac{6(n-1)}{n+2}}\right]. \quad (3.31)$$

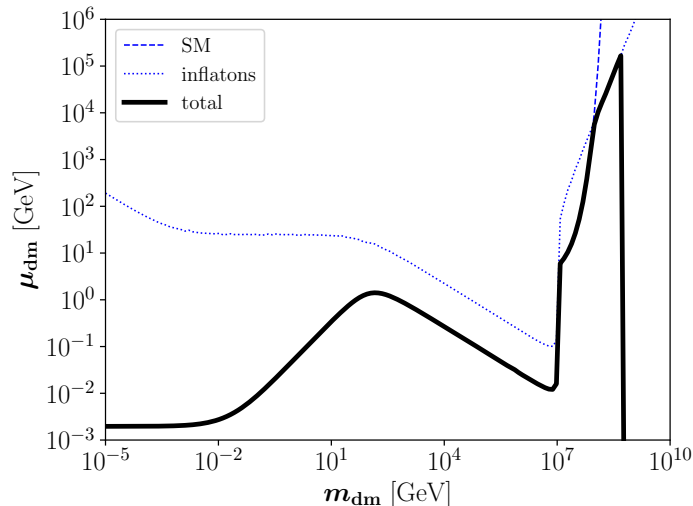


Figure 10. Parameter space that fits the whole observed DM abundance, for $n = 4$, $a_p/a_I = 10^5$, $a_t/a_I = 10^{10}$, $a_{\text{rh}}/a_I = 10^{15}$, $m_I = 10^{12}$ GeV and $H_I = 5 \times 10^8$ GeV, assuming production through annihilations from SM particles in the thermal bath (dashed blue), inflatons (dotted blue), gravitational production (sharp cut at $m_{\text{dm}} \simeq 2 \times 10^8$ GeV) and the combination (thick black).

Gravitation production from inflaton annihilation typically dominates over the annihilation from thermal-bath particles and can even overtake production through the exchange of S for very large values of H_I and m_{dm} .

Figure 10 is an example of the combination of all previously described DM production mechanisms, for $n = 4$, $a_p/a_I = 10^5$, $a_t/a_I = 10^{10}$, $a_{\text{rh}}/a_I = 10^{15}$, $m_I = 10^{12}$ GeV, and $H_I = 5 \times 10^8$ GeV. It shows the production through annihilations of SM particles in the thermal bath (dashed blue; see Fig. 7), inflatons (dotted blue; see Fig. 9), gravitational production (sharp cut at $m_{\text{dm}} \simeq 2 \times 10^8$ GeV), and the combination of all of them (thick black). For this particular choice of parameters, the production from the SM thermal bath dominates for low masses. The production from inflaton scatterings is comparable near the pole and dominates in a small region around $m_{\text{dm}} \sim 10^8$ GeV. For higher masses the gravitational production from inflaton annihilations dominates and overcloses the Universe for even higher DM masses. In summary, in this section, we find that, within the framework of resonance reheating, new features for DM UV freeze-in show up primarily due to the resonant temperature behavior near the pole.

4 Primordial gravitational waves

The resonant reheating scenario described so far can have a possible signature at the next-generation gravitational wave (GW) detectors, courtesy to the blue-tilted primordial GWs with an inflationary origin. In this section we discuss such a prospect.

The spectrum of GWs is described in terms of the fraction of their energy density per logarithmic wavenumber (frequency) k interval

$$\Omega_{\text{GW}}(a, k) = \frac{1}{\rho_c} \frac{d\rho_{\text{GW}}}{d \log k}, \quad (4.1)$$

normalized to the critical density $\rho_c = 3 H^2 M_P^2$. This expression can be recasted as [41, 84–86]

$$\Omega_{\text{GW}}(a, k) = \frac{1}{12} \left(\frac{k}{a H(a)} \right)^2 \mathcal{P}_{T, \text{prim}} \mathcal{T}(a, k), \quad (4.2)$$

where the primordial tensor power spectrum $\mathcal{P}_{T, \text{prim}}$ can be parametrized as [41, 86]

$$\mathcal{P}_{T, \text{prim}} = r \mathcal{P}_\zeta(k_\star) \left(\frac{k}{k_\star} \right)^{n_T}, \quad (4.3)$$

with $k_\star = 0.05 \text{ Mpc}^{-1}$ being the Planck pivot scale, $\mathcal{P}_\zeta(k_\star) \simeq 2.1 \times 10^{-9}$ [87] corresponding power spectrum of the scalar perturbation at the pivot scale, r is the tensor-to-scalar ratio and n_T represents the tensor spectral index. In single-field inflationary models, $n_T \simeq -r/8$. Considering the current bound on $r < 0.036$ [67], we set $n_T = 0$ throughout our analysis, which corresponds to a scale-invariant primordial spectrum. In Eq. (4.2) the transfer function $\mathcal{T}(a, k)$ connects primordial mode functions with mode functions at some later time as [86, 88]

$$\mathcal{T}(a, k) = \frac{1}{2} \left(\frac{a_{\text{hc}}}{a} \right)^2, \quad (4.4)$$

where the prefactor $1/2$ appears due to oscillation-averaging the tensor mode functions [86, 89, 90] and a_{hc} is scale factor at the horizon crossing defined as $a_{\text{hc}} H(a_{\text{hc}}) = k$. Different k modes might reenter the horizon at different epochs, i.e., during radiation domination or during reheating.

As is evident from Eq. (4.4), the transfer function characterizes the expansion history between the moment of horizon crossing $a = a_{\text{hc}}$ of a given mode k and some later moment $a > a_{\text{hc}}$. From Eq. (4.2), one can see that the spectral GW energy density at present (that is, at $a = a_0$) reads

$$\Omega_{\text{GW}}(k) \equiv \Omega_{\text{GW}}(a_0, k) = \frac{1}{24} \left(\frac{k}{a_0 H_0} \right)^2 \mathcal{P}_{T, \text{prim}} \left(\frac{a_{\text{hc}}}{a_0} \right)^2, \quad (4.5)$$

where H_0 is the Hubble expansion rate as measured today. Depending on the epoch of horizon re-entry for the perturbations, one can obtain the full GW spectral energy density as

$$\begin{aligned} \Omega_{\text{GW}}(a_{\text{hc}}) \simeq \Omega_\gamma^{(0)} \frac{\mathcal{P}_{T, \text{prim}}}{24} \frac{g_\star(T_{\text{hc}})}{2} \left(\frac{g_{\star s}(T_0)}{g_{\star s}(T_{\text{hc}})} \right)^{\frac{4}{3}} \\ \times \begin{cases} \frac{g_\star(T_{\text{rh}})}{g_\star(T_{\text{hc}})} \left(\frac{g_{\star s}(T_{\text{hc}})}{g_{\star s}(T_{\text{rh}})} \right)^{\frac{4}{3}} \left(\frac{a_{\text{rh}}}{a_{\text{hc}}} \right)^{\frac{2(n-4)}{n+2}} & \text{for } a_I < a_{\text{hc}} \leq a_{\text{rh}}, \\ 1 & \text{for } a_{\text{rh}} \leq a_{\text{hc}} \leq a_{\text{eq}}, \end{cases} \end{aligned} \quad (4.6)$$

where $\Omega_\gamma^{(0)} \equiv \rho_{\gamma, 0}/\rho_c = 2.47 \times 10^{-5} h^{-2}$ [72, 86] is the fraction of the energy density of photons at the present epoch and T_{hc} corresponds to the temperature at which the corresponding mode reenters the horizon. The first line holds for the modes that re-enter the horizon during reheating, while the second line applies for the modes re-entering after reheating, during the radiation-domination epoch. Note that, for $a_{\text{rh}} \leq a_{\text{hc}} \leq a_{\text{eq}}$, we have assumed conservation of entropy from the moment of horizon crossing until today, implying $T \propto a^{-1} g_{\star s}^{-1/3}$, with

$a = a_{\text{eq}}$ being the scale factor at the matter-radiation equivalence at $T \equiv T_{\text{eq}} \simeq 0.7$ eV. The corresponding GW frequency f can be expressed as

$$f(a_{\text{hc}}) \equiv \frac{k}{2\pi a_0} = \frac{1}{6} \sqrt{\frac{g_\star(T_{\text{rh}})}{10}} \left(\frac{g_{\star s}(T_0)}{g_{\star s}(T_{\text{rh}})} \right)^{\frac{1}{3}} \frac{T_0 T_{\text{rh}}}{M_P} \times \begin{cases} \left(\frac{a_{\text{rh}}}{a_{\text{hc}}} \right)^{\frac{2(n-1)}{n+2}} & \text{for } a_I < a_{\text{hc}} \leq a_{\text{rh}}, \\ \frac{a_{\text{rh}}}{a_{\text{hc}}} & \text{for } a_{\text{rh}} \leq a_{\text{hc}} \leq a_{\text{eq}}, \end{cases} \quad (4.7)$$

with $T_0 \simeq 2.3 \times 10^{-13}$ GeV [71]. Combining Eqs. (4.6) and (4.7) we can rewrite the GR spectrum as a function of the frequency

$$\Omega_{\text{GW}}(f) \simeq \Omega_\gamma^{(0)} \frac{\mathcal{P}_{T,\text{prim}}}{24} \frac{g_\star(T_{\text{hc}})}{2} \left(\frac{g_{\star s}(T_0)}{g_{\star s}(T_{\text{hc}})} \right)^{\frac{4}{3}} \times \begin{cases} \frac{g_\star(T_{\text{rh}})}{g_\star(T_{\text{hc}})} \left(\frac{g_{\star s}(T_{\text{hc}})}{g_{\star s}(T_{\text{rh}})} \right)^{\frac{4}{3}} \left(\frac{f}{f_{\text{rh}}} \right)^{\frac{n-4}{n-1}} & \text{for } f_{\text{rh}} \leq f < f_{\text{max}}, \\ 1 & \text{for } f_{\text{eq}} \leq f \leq f_{\text{rh}}, \end{cases} \quad (4.8)$$

where $f_{\text{eq}} \equiv f(a_{\text{eq}})$ and

$$f(a_{\text{rh}}) \equiv \frac{1}{6} \sqrt{\frac{g_\star(T_{\text{rh}})}{10}} \left(\frac{g_{\star s}(T_0)}{g_{\star s}(T_{\text{rh}})} \right)^{\frac{1}{3}} \frac{T_0 T_{\text{rh}}}{M_P}. \quad (4.9)$$

Finally, the GW spectrum presents a cutoff in frequency corresponding to $a_{\text{hc}} = a_I$,

$$f_{\text{max}} \equiv \frac{H_I}{2\pi} \frac{a_I}{a_0} = \frac{H_I}{2\pi} \left(\frac{g_{\star s}(T_0)}{g_{\star s}(T_{\text{rh}})} \right)^{\frac{1}{3}} \frac{a_I}{a_{\text{rh}}} \frac{T_0}{T_{\text{rh}}}. \quad (4.10)$$

From Eq. (4.8) one can see that modes that reenter the horizon after reheating (that is $f < f_{\text{rh}}$) keep the same dependence with the frequency as the original primordial spectrum $\mathcal{P}_{T,\text{prim}}$. However, if they reenter during reheating ($f_{\text{rh}} < f < f_{\text{max}}$), $\Omega_{\text{GW}}(f)$ gets a boost $\propto f^{\frac{n-4}{n-1}}$, which implies that the spectrum becomes blue tilted with respect to the primordial one. Interestingly, this only happens for $n > 4$, as for $n = 4$ the Universe scales as free radiation during (and after) reheating.

In Fig. 11, we show the GW spectral energy density at present epoch, as a function of the frequency f for $a_{\text{rh}}/a_I = 10^3$ (left) and $a_{\text{rh}}/a_I = 10^{10}$ (right), and three choices of the inflaton potential: $n = 4$ (solid black), $n = 6$ (dashed black) and $n = 8$ (dashed-dotted black). We also used $H_I = 2 \times 10^{13}$ GeV and the maximum value for the tensor-to-scalar ratio $r = 0.035$ [67]. We overlaid in yellow projected sensitivity curves from the Big Bang Observer (BBO) [91, 92], ultimate DECIGO [93, 94], LISA [95], μAres [96], the cosmic explorer (CE) [97], the Einstein Telescope (ET) [98–101], and from resonant cavities [102], see Ref. [103] for a recent review. In all cases, the GW energy density is safe from the constraint on ΔN_{eff} [87], which quantifies the extra radiation-like degrees of freedom around BBN. Note that for a larger a_{rh}/a_I (right panel) the GW spectrum receives a larger boost because in that case the reheating lasts longer, resulting in a longer stiff epoch that contributes to the blue tilt. As a consequence, the spectrum falls within the sensitivity of not only the high-frequency detectors like resonant

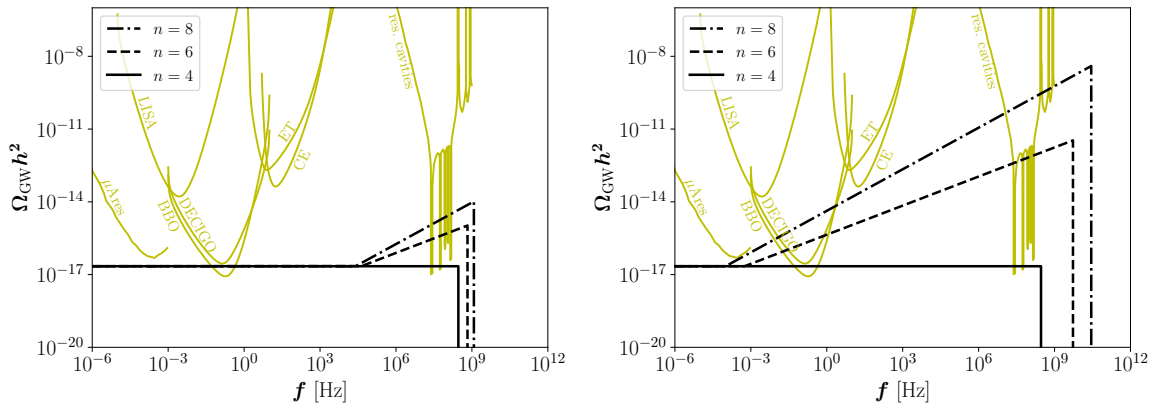


Figure 11. Gravitational wave spectral energy density $\Omega_{\text{GW}}h^2$ as function of the frequency f , and $n = 4$, $n = 6$ or $n = 8$. The left panel corresponds to $a_{\text{rh}}/a_I = 10^3$, while the right panel corresponds to $a_{\text{rh}}/a_I = 10^{10}$. In the figure $H_I = 2 \times 10^{13}$ GeV and $r = 0.035$. The yellow lines correspond to projected sensitivities of different detectors.

cavity but also low-frequency detectors like BBO and DECIGO. We emphasize that although such a spectrum is not unique to resonant reheating scenario (and can be generic to any stiff background in the early Universe), any potential signal of primordial GW either in the low or in the high frequencies can not rule out the possibility of resonant production of radiation bath.

5 Conclusions

In this study, we investigate a reheating scenario where the transfer of energy from the inflaton ϕ to the Standard Model (SM) particles proceeds through an s -channel mediated scattering. We consider the inflaton to oscillate around a generic monomial potential $\propto \phi^n$, with the inflaton mass m_ϕ being field dependent and therefore varying over time if $n > 2$. If the mediator mass m_s is of the order of the inflaton mass m_ϕ , a *resonance* can develop during reheating once the inflaton mass is $m_\phi(\phi) \simeq m_s/2$. We validate these characteristics by solving a system of coupled Boltzmann equations for the inflaton and SM energy densities (Eqs. (2.2) and (2.3)) and observe a characteristic bump occurring both in the radiation and in the temperature profiles, as depicted in Fig. 1. Furthermore, we derive several analytical approximations, detailed in Eq. (2.13), which nicely fits the numerical results. Our investigation reveals that resonance reheating exhibits more nuanced temperature scaling compared to conventional scenarios presented in the existing literature, which is typically characterized by a featureless power law, as given in Eq. (2.20). In scenarios where the mediator is always heavier than the inflaton, precluding the development of resonance, our model successfully reproduces the results of the existing literature. Alternatively, when the mediator is always lighter than the inflaton, the SM temperature rises throughout the reheating phase, with the reheating temperature serving as the maximum temperature achieved; see Fig. 3.

Some implications for particle phenomenology and cosmology during resonant reheating were studied. First, the mediator could play a pivotal role in producing not only the SM states but also particles beyond the SM, such as dark matter (DM). If the interaction rates between the DM and the visible sector are very suppressed, DM could be produced during reheating

through the annihilation of a pair of SM or inflaton particles. Similarly to radiation, DM production also has a very rich freeze-in phenomenology, as illustrated in Figs. 6, 8, and 10.

Second, we also proposed the prospect of finding a signature of this model via the primordial gravitational wave (GW) spectrum. For $n > 4$, the inflationary GW spectrum experiences a significant blue tilt within the frequency range corresponding to the modes that cross the horizon during the stiff period. The resulting spectrum could be well within the reach of several next-generation low- and high-frequency GW detectors, as shown in Fig. 11.

Acknowledgments

NB received funding from the Spanish FEDER / MCIU-AEI under the grant FPA2017-84543-P. YX acknowledges the support from the Cluster of Excellence ‘‘Precision Physics, Fundamental Interactions, and Structure of Matter’’ (PRISMA⁺ EXC 2118/1) funded by the Deutsche Forschungsgemeinschaft (DFG, German Research Foundation) within the German Excellence Strategy (Project No. 390831469).

A Annihilation to mediators

In our setup, the annihilation $\phi\phi \rightarrow ss$ through a t - and u -channel exchange of a ϕ is also kinematically open. We assume that s particles have a sufficiently large decay width and rapidly decay into SM radiation once they are produced. The total production rate considering the t and u channels is

$$\Gamma^{\phi\phi \rightarrow ss} \simeq \frac{\rho_\phi}{m_\phi} \frac{1}{16\pi m_\phi^2} \left(\frac{\mu_\phi^2}{m_s^2 - 2m_\phi^2} \right)^2 \sqrt{1 - \frac{m_s^2}{m_\phi^2}}. \quad (\text{A.1})$$

The solution for the radiation energy density is

$$\rho_R(a) \simeq \frac{9}{64\pi} \frac{n}{8n - 17} \left(\frac{a}{a_I} \right)^{\frac{6(2n-7)}{2+n}} \left[1 - \left(\frac{a_I}{a} \right)^{\frac{2(8n-17)}{2+n}} \right] \frac{H_I^3 M_P^4 \mu_\phi^4}{M_I^7} \quad (\text{A.2})$$

in the limit $m_s \ll m_\phi$. Note that if $\mu_h = \mu_\phi$, Eq. (A.2) and the first line of Eq. (2.13) are the same (up to a factor 8), making this channel potentially important. However, if one demands an extended reheating period, a long-lived inflaton is desirable, and hence a suppressed μ_ϕ . Under these circumstances, the inflaton annihilation into mediators is suppressed. We have checked that in all the benchmarks used in this work, this channel is completely subdominant.

References

- [1] A.A. Starobinsky, *A New Type of Isotropic Cosmological Models Without Singularity*, *Phys. Lett. B* **91** (1980) 99.
- [2] A.H. Guth, *The Inflationary Universe: A Possible Solution to the Horizon and Flatness Problems*, *Phys. Rev. D* **23** (1981) 347.
- [3] A.D. Linde, *A New Inflationary Universe Scenario: A Possible Solution of the Horizon, Flatness, Homogeneity, Isotropy and Primordial Monopole Problems*, *Phys. Lett. B* **108** (1982) 389.
- [4] A. Albrecht and P.J. Steinhardt, *Cosmology for Grand Unified Theories with Radiatively Induced Symmetry Breaking*, *Phys. Rev. Lett.* **48** (1982) 1220.

- [5] L.F. Abbott, E. Farhi and M.B. Wise, *Particle Production in the New Inflationary Cosmology*, *Phys. Lett. B* **117** (1982) 29.
- [6] L. Kofman, A.D. Linde and A.A. Starobinsky, *Reheating after inflation*, *Phys. Rev. Lett.* **73** (1994) 3195 [[hep-th/9405187](#)].
- [7] L. Kofman, A.D. Linde and A.A. Starobinsky, *Towards the theory of reheating after inflation*, *Phys. Rev. D* **56** (1997) 3258 [[hep-ph/9704452](#)].
- [8] J.F. Dufaux, G.N. Felder, L. Kofman, M. Peloso and D. Podolsky, *Preheating with trilinear interactions: Tachyonic resonance*, *JCAP* **07** (2006) 006 [[hep-ph/0602144](#)].
- [9] K.D. Lozanov, *Lectures on Reheating after Inflation*, [1907.04402](#).
- [10] M.A.G. García, K. Kaneta, Y. Mambrini and K.A. Olive, *Inflaton Oscillations and Post-Inflationary Reheating*, *JCAP* **04** (2021) 012 [[2012.10756](#)].
- [11] N. Bernal, S. Cléry, Y. Mambrini and Y. Xu, *Probing reheating with graviton bremsstrahlung*, *JCAP* **01** (2024) 065 [[2311.12694](#)].
- [12] M.A.G. García, K. Kaneta, Y. Mambrini and K.A. Olive, *Reheating and Post-inflationary Production of Dark Matter*, *Phys. Rev. D* **101** (2020) 123507 [[2004.08404](#)].
- [13] R.T. Co, E. González and K. Harigaya, *Increasing Temperature toward the Completion of Reheating*, *JCAP* **11** (2020) 038 [[2007.04328](#)].
- [14] A. Ahmed, B. Grzadkowski and A. Socha, *Implications of time-dependent inflaton decay on reheating and dark matter production*, *Phys. Lett. B* **831** (2022) 137201 [[2111.06065](#)].
- [15] P. Arias, N. Bernal, J.K. Osiński and L. Roszkowski, *Dark matter axions in the early universe with a period of increasing temperature*, *JCAP* **05** (2023) 028 [[2207.07677](#)].
- [16] B. Barman, N. Bernal, Y. Xu and Ó. Zapata, *Ultraviolet freeze-in with a time-dependent inflaton decay*, *JCAP* **07** (2022) 019 [[2202.12906](#)].
- [17] S. Cléry, Y. Mambrini, K.A. Olive and S. Verner, *Gravitational portals in the early Universe*, *Phys. Rev. D* **105** (2022) 075005 [[2112.15214](#)].
- [18] M.R. Haque and D. Maity, *Gravitational reheating*, *Phys. Rev. D* **107** (2023) 043531 [[2201.02348](#)].
- [19] R.T. Co, Y. Mambrini and K.A. Olive, *Inflationary gravitational leptogenesis*, *Phys. Rev. D* **106** (2022) 075006 [[2205.01689](#)].
- [20] B. Barman, S. Cléry, R.T. Co, Y. Mambrini and K.A. Olive, *Gravity as a portal to reheating, leptogenesis and dark matter*, *JHEP* **12** (2022) 072 [[2210.05716](#)].
- [21] M.R. Haque, D. Maity and R. Mondal, *Gravitational neutrino reheating*, *Phys. Rev. D* **109** (2024) 063543 [[2311.07684](#)].
- [22] S. Cléry, Y. Mambrini, K.A. Olive, A. Shkerin and S. Verner, *Gravitational portals with nonminimal couplings*, *Phys. Rev. D* **105** (2022) 095042 [[2203.02004](#)].
- [23] B. Barman, N. Bernal and J. Rubio, *Rescuing Gravitational-Reheating in Chaotic Inflation*, [2310.06039](#).
- [24] J. McDonald, *Thermally generated gauge singlet scalars as selfinteracting dark matter*, *Phys. Rev. Lett.* **88** (2002) 091304 [[hep-ph/0106249](#)].
- [25] K.-Y. Choi and L. Roszkowski, *E-WIMPs*, *AIP Conf. Proc.* **805** (2005) 30 [[hep-ph/0511003](#)].
- [26] A. Kusenko, *Sterile neutrinos, dark matter, and the pulsar velocities in models with a Higgs singlet*, *Phys. Rev. Lett.* **97** (2006) 241301 [[hep-ph/0609081](#)].
- [27] K. Petraki and A. Kusenko, *Dark-matter sterile neutrinos in models with a gauge singlet in the Higgs sector*, *Phys. Rev. D* **77** (2008) 065014 [[0711.4646](#)].

- [28] L.J. Hall, K. Jedamzik, J. March-Russell and S.M. West, *Freeze-In Production of FIMP Dark Matter*, *JHEP* **03** (2010) 080 [[0911.1120](#)].
- [29] N. Bernal, M. Heikinheimo, T. Tenkanen, K. Tuominen and V. Vaskonen, *The Dawn of FIMP Dark Matter: A Review of Models and Constraints*, *Int. J. Mod. Phys. A* **32** (2017) 1730023 [[1706.07442](#)].
- [30] F. Elahi, C. Kolda and J. Unwin, *UltraViolet Freeze-in*, *JHEP* **03** (2015) 048 [[1410.6157](#)].
- [31] M.A.G. García, Y. Mambrini, K.A. Olive and M. Peloso, *Enhancement of the Dark Matter Abundance Before Reheating: Applications to Gravitino Dark Matter*, *Phys. Rev. D* **96** (2017) 103510 [[1709.01549](#)].
- [32] N. Bernal, F. Elahi, C. Maldonado and J. Unwin, *Ultraviolet Freeze-in and Non-Standard Cosmologies*, *JCAP* **11** (2019) 026 [[1909.07992](#)].
- [33] R. Allahverdi et al., *The First Three Seconds: a Review of Possible Expansion Histories of the Early Universe*, *Open J.Astrophys.* **4** (2021) [[2006.16182](#)].
- [34] M. Giovannini, *Gravitational waves constraints on postinflationary phases stiffer than radiation*, *Phys. Rev. D* **58** (1998) 083504 [[hep-ph/9806329](#)].
- [35] A. Riazuelo and J.-P. Uzan, *Quintessence and gravitational waves*, *Phys. Rev. D* **62** (2000) 083506 [[astro-ph/0004156](#)].
- [36] N. Seto and J. Yokoyama, *Probing the equation of state of the early universe with a space laser interferometer*, *J. Phys. Soc. Jap.* **72** (2003) 3082 [[gr-qc/0305096](#)].
- [37] L.A. Boyle and A. Buonanno, *Relating gravitational wave constraints from primordial nucleosynthesis, pulsar timing, laser interferometers, and the CMB: Implications for the early Universe*, *Phys. Rev. D* **78** (2008) 043531 [[0708.2279](#)].
- [38] A. Stewart and R. Brandenberger, *Observational Constraints on Theories with a Blue Spectrum of Tensor Modes*, *JCAP* **08** (2008) 012 [[0711.4602](#)].
- [39] B. Li and P.R. Shapiro, *Precision cosmology and the stiff-amplified gravitational-wave background from inflation: NANOGrav, Advanced LIGO-Virgo and the Hubble tension*, *JCAP* **10** (2021) 024 [[2107.12229](#)].
- [40] M. Artymowski, O. Czerwińska, Z. Lalak and M. Lewicki, *Gravitational wave signals and cosmological consequences of gravitational reheating*, *JCAP* **04** (2018) 046 [[1711.08473](#)].
- [41] C. Caprini and D.G. Figueroa, *Cosmological Backgrounds of Gravitational Waves*, *Class. Quant. Grav.* **35** (2018) 163001 [[1801.04268](#)].
- [42] N. Bernal and F. Hajkarim, *Primordial Gravitational Waves in Nonstandard Cosmologies*, *Phys. Rev. D* **100** (2019) 063502 [[1905.10410](#)].
- [43] D.G. Figueroa and E.H. Tanin, *Ability of LIGO and LISA to probe the equation of state of the early Universe*, *JCAP* **08** (2019) 011 [[1905.11960](#)].
- [44] T. Opferkuch, P. Schwaller and B.A. Stefanek, *Ricci Reheating*, *JCAP* **07** (2019) 016 [[1905.06823](#)].
- [45] N. Bernal, A. Ghoshal, F. Hajkarim and G. Lambiase, *Primordial Gravitational Wave Signals in Modified Cosmologies*, *JCAP* **11** (2020) 051 [[2008.04959](#)].
- [46] Y. Gouttenoire, G. Servant and P. Simakachorn, *Kination cosmology from scalar fields and gravitational-wave signatures*, [2111.01150](#).
- [47] R. Caldwell et al., *Detection of early-universe gravitational-wave signatures and fundamental physics*, *Gen. Rel. Grav.* **54** (2022) 156 [[2203.07972](#)].

- [48] A. Chakraborty, M.R. Haque, D. Maity and R. Mondal, *Inflaton phenomenology via reheating in light of primordial gravitational waves and the latest BICEP/Keck data*, *Phys. Rev. D* **108** (2023) 023515 [[2304.13637](#)].
- [49] B. Barman, A. Ghoshal, B. Grzadkowski and A. Socha, *Measuring inflaton couplings via primordial gravitational waves*, *JHEP* **07** (2023) 231 [[2305.00027](#)].
- [50] B. Barman, S. Jyoti Das, M.R. Haque and Y. Mambrini, *A Gravitational Ménage à Trois: leptogenesis, primordial gravitational wave & PBH-induced reheating*, [2403.05626](#).
- [51] R. Kallosh and A. Linde, *Universality Class in Conformal Inflation*, *JCAP* **07** (2013) 002 [[1306.5220](#)].
- [52] R. Kallosh, A. Linde and D. Roest, *Superconformal Inflationary α -Attractors*, *JHEP* **11** (2013) 198 [[1311.0472](#)].
- [53] A.A. Starobinsky, *Nonsingular Model of the Universe with the Quantum Gravitational de Sitter Stage and its Observational Consequences*, in *Second Seminar on Quantum Gravity*, 1981.
- [54] A.A. Starobinsky, *The Perturbation Spectrum Evolving from a Nonsingular Initially De-Sitter Cosmology and the Microwave Background Anisotropy*, *Sov. Astron. Lett.* **9** (1983) 302.
- [55] L.A. Kofman, A.D. Linde and A.A. Starobinsky, *Inflationary Universe Generated by the Combined Action of a Scalar Field and Gravitational Vacuum Polarization*, *Phys. Lett. B* **157** (1985) 361.
- [56] M.S. Turner, *Coherent Scalar Field Oscillations in an Expanding Universe*, *Phys. Rev. D* **28** (1983) 1243.
- [57] J. Ellis, M.A.G. García, D.V. Nanopoulos, K.A. Olive and M. Peloso, *Post-Inflationary Gravitino Production Revisited*, *JCAP* **03** (2016) 008 [[1512.05701](#)].
- [58] K. Harigaya and K. Mukaida, *Thermalization after/during Reheating*, *JHEP* **05** (2014) 006 [[1312.3097](#)].
- [59] M.A.G. García and M.A. Amin, *Prethermalization production of dark matter*, *Phys. Rev. D* **98** (2018) 103504 [[1806.01865](#)].
- [60] M. Drees and B. Najjari, *Energy spectrum of thermalizing high energy decay products in the early universe*, *JCAP* **10** (2021) 009 [[2105.01935](#)].
- [61] M. Drees and B. Najjari, *Multi-species thermalization cascade of energetic particles in the early universe*, *JCAP* **08** (2023) 037 [[2205.07741](#)].
- [62] N. Bernal and Y. Xu, *WIMPs during reheating*, *JCAP* **12** (2022) 017 [[2209.07546](#)].
- [63] Y. Shtanov, J.H. Traschen and R.H. Brandenberger, *Universe reheating after inflation*, *Phys. Rev. D* **51** (1995) 5438 [[hep-ph/9407247](#)].
- [64] K. Ichikawa, T. Suyama, T. Takahashi and M. Yamaguchi, *Primordial Curvature Fluctuation and Its Non-Gaussianity in Models with Modulated Reheating*, *Phys. Rev. D* **78** (2008) 063545 [[0807.3988](#)].
- [65] K. Kainulainen, S. Nurmi, T. Tenkanen, K. Tuominen and V. Vaskonen, *Isocurvature Constraints on Portal Couplings*, *JCAP* **06** (2016) 022 [[1601.07733](#)].
- [66] B. Barman, N. Bernal, Y. Xu and Ó. Zapata, *Bremsstrahlung-induced gravitational waves in monomial potentials during reheating*, *Phys. Rev. D* **108** (2023) 083524 [[2305.16388](#)].
- [67] BICEP, KECK collaboration, *Improved Constraints on Primordial Gravitational Waves using Planck, WMAP, and BICEP/Keck Observations through the 2018 Observing Season*, *Phys. Rev. Lett.* **127** (2021) 151301 [[2110.00483](#)].
- [68] B. Barman and N. Bernal, *Gravitational SIMPs*, *JCAP* **06** (2021) 011 [[2104.10699](#)].

- [69] G.F. Giudice, E.W. Kolb and A. Riotto, *Largest temperature of the radiation era and its cosmological implications*, *Phys. Rev. D* **64** (2001) 023508 [[hep-ph/0005123](#)].
- [70] Y. Xu, *Constraining axion and ALP dark matter from misalignment during reheating*, *Phys. Rev. D* **108** (2023) 083536 [[2308.15322](#)].
- [71] PARTICLE DATA GROUP collaboration, *Review of Particle Physics*, *PTEP* **2022** (2022) 083C01.
- [72] PLANCK collaboration, *Planck 2018 results. VI. Cosmological parameters*, *Astron. Astrophys.* **641** (2020) A6 [[1807.06209](#)].
- [73] J. Silva-Malpartida, N. Bernal, J. Jones-Pérez and R.A. Lineros, *From WIMPs to FIMPs with low reheating temperatures*, *JCAP* **09** (2023) 015 [[2306.14943](#)].
- [74] M. Becker, E. Copello, J. Harz, J. Lang and Y. Xu, *Confronting dark matter freeze-in during reheating with constraints from inflation*, *JCAP* **01** (2024) 053 [[2306.17238](#)].
- [75] C. Cosme, F. Costa and O. Lebedev, *Freeze-in at stronger coupling*, [2306.13061](#).
- [76] C. Cosme, F. Costa and O. Lebedev, *Temperature evolution in the Early Universe and freeze-in at stronger coupling*, [2402.04743](#).
- [77] M. Garny, M. Sandora and M.S. Sloth, *Planckian Interacting Massive Particles as Dark Matter*, *Phys. Rev. Lett.* **116** (2016) 101302 [[1511.03278](#)].
- [78] M. Garny, A. Palessandro, M. Sandora and M.S. Sloth, *Theory and Phenomenology of Planckian Interacting Massive Particles as Dark Matter*, *JCAP* **02** (2018) 027 [[1709.09688](#)].
- [79] Y. Tang and Y.-L. Wu, *On Thermal Gravitational Contribution to Particle Production and Dark Matter*, *Phys. Lett. B* **774** (2017) 676 [[1708.05138](#)].
- [80] N. Bernal, M. Dutra, Y. Mambrini, K. Olive, M. Peloso and M. Pierre, *Spin-2 Portal Dark Matter*, *Phys. Rev. D* **97** (2018) 115020 [[1803.01866](#)].
- [81] Y. Mambrini and K.A. Olive, *Gravitational Production of Dark Matter during Reheating*, *Phys. Rev. D* **103** (2021) 115009 [[2102.06214](#)].
- [82] N. Bernal and C.S. Fong, *Dark matter and leptogenesis from gravitational production*, *JCAP* **06** (2021) 028 [[2103.06896](#)].
- [83] N. Bernal, J. Harz, M. Mojahed and Y. Xu, *Dark Matter Production in Large Field Inflation*, [2407. soon](#).
- [84] M. Maggiore, *Gravitational wave experiments and early universe cosmology*, *Phys. Rept.* **331** (2000) 283 [[gr-qc/9909001](#)].
- [85] Y. Watanabe and E. Komatsu, *Improved Calculation of the Primordial Gravitational Wave Spectrum in the Standard Model*, *Phys. Rev. D* **73** (2006) 123515 [[astro-ph/0604176](#)].
- [86] K. Saikawa and S. Shirai, *Primordial gravitational waves, precisely: The role of thermodynamics in the Standard Model*, *JCAP* **05** (2018) 035 [[1803.01038](#)].
- [87] PLANCK collaboration, *Planck 2018 results. X. Constraints on inflation*, *Astron. Astrophys.* **641** (2020) A10 [[1807.06211](#)].
- [88] L.A. Boyle and P.J. Steinhardt, *Probing the early universe with inflationary gravitational waves*, *Phys. Rev. D* **77** (2008) 063504 [[astro-ph/0512014](#)].
- [89] D.G. Figueroa and E.H. Tanin, *Inconsistency of an inflationary sector coupled only to Einstein gravity*, *JCAP* **10** (2019) 050 [[1811.04093](#)].
- [90] G. Choi, R. Jinno and T.T. Yanagida, *Probing PeV scale SUSY breaking with satellite galaxies and primordial gravitational waves*, *Phys. Rev. D* **104** (2021) 095018 [[2107.12804](#)].

- [91] J. Crowder and N.J. Cornish, *Beyond LISA: Exploring future gravitational wave missions*, *Phys. Rev. D* **72** (2005) 083005 [[gr-qc/0506015](#)].
- [92] V. Corbin and N.J. Cornish, *Detecting the cosmic gravitational wave background with the big bang observer*, *Class. Quant. Grav.* **23** (2006) 2435 [[gr-qc/0512039](#)].
- [93] N. Seto, S. Kawamura and T. Nakamura, *Possibility of direct measurement of the acceleration of the universe using 0.1-Hz band laser interferometer gravitational wave antenna in space*, *Phys. Rev. Lett.* **87** (2001) 221103 [[astro-ph/0108011](#)].
- [94] H. Kudoh, A. Taruya, T. Hiramatsu and Y. Himemoto, *Detecting a gravitational-wave background with next-generation space interferometers*, *Phys. Rev. D* **73** (2006) 064006 [[gr-qc/0511145](#)].
- [95] LISA collaboration, *Laser Interferometer Space Antenna*, [1702.00786](#).
- [96] A. Sesana et al., *Unveiling the gravitational universe at μ -Hz frequencies*, *Exper. Astron.* **51** (2021) 1333 [[1908.11391](#)].
- [97] D. Reitze et al., *Cosmic Explorer: The U.S. Contribution to Gravitational-Wave Astronomy beyond LIGO*, *Bull. Am. Astron. Soc.* **51** (2019) 035 [[1907.04833](#)].
- [98] S. Hild et al., *Sensitivity Studies for Third-Generation Gravitational Wave Observatories*, *Class. Quant. Grav.* **28** (2011) 094013 [[1012.0908](#)].
- [99] M. Punturo et al., *The Einstein Telescope: A third-generation gravitational wave observatory*, *Class. Quant. Grav.* **27** (2010) 194002.
- [100] B. Sathyaprakash et al., *Scientific Objectives of Einstein Telescope*, *Class. Quant. Grav.* **29** (2012) 124013 [[1206.0331](#)].
- [101] M. Maggiore et al., *Science Case for the Einstein Telescope*, *JCAP* **03** (2020) 050 [[1912.02622](#)].
- [102] N. Herman, L. Lehoucq and A. Fúzfa, *Electromagnetic antennas for the resonant detection of the stochastic gravitational wave background*, *Phys. Rev. D* **108** (2023) 124009 [[2203.15668](#)].
- [103] N. Aggarwal et al., *Challenges and opportunities of gravitational-wave searches at MHz to GHz frequencies*, *Living Rev. Rel.* **24** (2021) 4 [[2011.12414](#)].